Cell



# *Streptococcus anginosus* promotes gastric inflammation, atrophy, and tumorigenesis in mice

## Graphical abstract

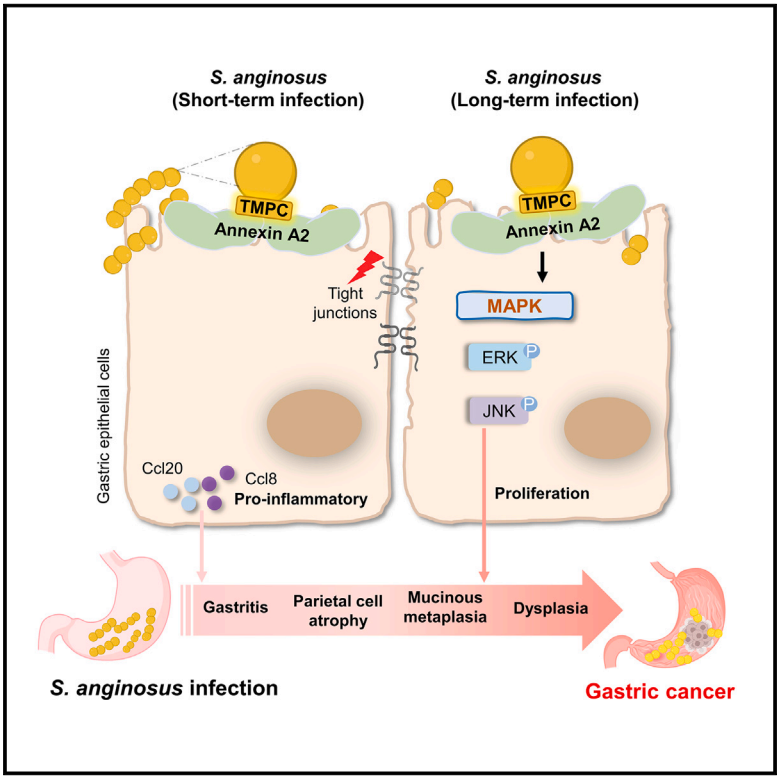


## Authors

Kaili Fu, Alvin Ho Kwan Cheung, Chi Chun Wong, ..., Ka Fai To, Joseph Jao Yiu Sung, Jun Yu

## Correspondence

josephsung@ntu.edu.sg (J.J.Y.S.), junyu@cuhk.edu.hk (J.Y.)

## In brief

Gastric cancer has been usually linked to the bacterium *Helicobacter pylori*. Here, the authors identify *Streptococcus anginosus* as a pathogen that promotes gastric tumorigenesis through its surface protein TMPC binding through an Annexin-2 and MAPK signaling cascade.

## Highlights

- *S. anginosus* is enriched in the gastric mucosa of patients with GC
- *S. anginosus* induces gastritis-atrophy-metaplasia-dysplasia sequence in mice
- *S. anginosus* promotes gastric tumorigenesis
- TMPC-Annexin A2 axis mediates *S. anginosus* colonization and activates MAPK signaling

Fu et al., 2024, Cell *187*, 882–896
February 15, 2024 
https://doi.org/10.1016/j.cell.2024.01.004

CellPress

CellPress
OPEN ACCESS

Cell

Article

# *Streptococcus anginosus* promotes gastric inflammation, atrophy, and tumorigenesis in mice

Kaili Fu,[1] Alvin Ho Kwan Cheung,[2] Chi Chun Wong,[1] Weixin Liu,[1] Yunfei Zhou,[1] Feixue Wang,[1] Pingmei Huang,[1] Kai Yuan,[1] Olabisi Oluwabukola Coker,[1] Yasi Pan,[1] Danyu Chen,[1] Nga Man Lam,[3] Mengxue Gao,[4] Xiang Zhang,[1] He Huang,[4] Ka Fai To,[2] Joseph Jao Yiu Sung,[1,5,*] and Jun Yu[1,6,*]

[1]Institute of Digestive Disease and Department of Medicine and Therapeutics, State Key Laboratory of Digestive Disease, Li Ka Shing Institute of Health Sciences, The Chinese University of Hong Kong, Hong Kong SAR, China
[2]Department of Anatomical and Cellular Pathology, The Chinese University of Hong Kong, Hong Kong SAR, China
[3]Department of Microbiology, The Chinese University of Hong Kong, Hong Kong SAR, China
[4]Department of Biochemical Engineering, School of Chemical Engineering and Technology, Tianjin University, Tianjin, China
[5]Lee Kong Chian School of Medicine, Nanyang Technological University, Singapore, Singapore
[6]Lead contact
*Correspondence: josephsung@ntu.edu.sg (J.J.Y.S.), junyu@cuhk.edu.hk (J.Y.)
https://doi.org/10.1016/j.cell.2024.01.004

## SUMMARY

*Streptococcus anginosus* (*S. anginosus*) was enriched in the gastric mucosa of patients with gastric cancer (GC). Here, we show that *S. anginosus* colonized the mouse stomach and induced acute gastritis. *S. anginosus* infection spontaneously induced progressive chronic gastritis, parietal cell atrophy, mucinous metaplasia, and dysplasia in conventional mice, and the findings were confirmed in germ-free mice. In addition, *S. anginosus* accelerated GC progression in carcinogen-induced gastric tumorigenesis and YTN16 GC cell allografts. Consistently, *S. anginosus* disrupted gastric barrier function, promoted cell proliferation, and inhibited apoptosis. Mechanistically, we identified an *S. anginosus* surface protein, TMPC, that interacts with Annexin A2 (ANXA2) receptor on gastric epithelial cells. Interaction of TMPC with ANXA2 mediated attachment and colonization of *S. anginosus* and induced mitogen-activated protein kinase (MAPK) activation. ANXA2 knockout abrogated the induction of MAPK by *S. anginosus*. Thus, this study reveals *S. anginosus* as a pathogen that promotes gastric tumorigenesis via direct interactions with gastric epithelial cells in the TMPC-ANXA2-MAPK axis.

## INTRODUCTION

Gastric cancer (GC) is the fifth most common cancer and a leading cause of cancer mortality worldwide.[1] *Helicobacter pylori* (*H. pylori*), a major risk factor for GC, has been classified as a type I carcinogen. *H. pylori* infection promotes gastritis, atrophy, and intestinal metaplasia (IM).[2] Among *H. pylori*-infected individuals, only 1%–3% eventually develop GC, inferring the involvement of other contributing factors. Emerging evidence indicates the presence of a substantial number of non-*H. pylori* microbiome residing in the gastric mucosa,[3] and their deregulation might play a role in gastric carcinogenesis.[4] Nevertheless, the identification and characterization of non-*H. pylori* driver bacteria associated with gastric carcinogenesis remain unexplored.

To explore the non-*H. pylori* gastric microbiome, we characterized the gastric microbiome of *H. pylori*-negative patients through the different stages of gastric tumorigenesis from superficial gastritis, atrophic gastritis, and IM to GC, leading to the discovery of five oral pathogens that were enriched in GC, including *Streptococcus anginosus* (*S. anginosus*).[5] *S. anginosus* is a gram-positive, non-spore-forming, nonmotile bacterium[6] that primarily resides in the oral cavity, nasopharynx, gastrointestinal tract, and vaginal tract, and it can cause invasive pyogenic infections like abscesses.[7] *S. anginosus* is markedly resilient to low pH conditions (pH 3–5), which might facilitate its survival in the gastric mucosa.[8] However, the role of *S. anginosus* in gastric carcinogenesis and its pathogenic molecular mechanisms are largely unclear.

In this study, *S. anginosus* was identified as a non-*H. pylori* pathogen that rapidly induces acute gastritis and consequently chronic gastritis, gastric mucinous metaplasia, and dysplasia in conventional mice and germ-free mice following long-term infection. *S. anginosus* accelerates gastric carcinogenesis. Mechanistically, we revealed that the *S. anginosus* surface protein TMPC directly interacts with gastric epithelial cell receptor Annexin A2 (ANXA2) for its colonization in gastric mucosa, which, in turn, mediates the activation of mitogen-activated protein kinases (MAPK) signaling pathway. Hence, our study defined a non-*H. pylori* pathogen, *S. anginosus*, that directly contributes to gastric tumorigenesis.

 

## RESULTS

### *S. anginosus* induces acute gastritis in mice following 2 weeks of infection

We initially analyzed *S. anginosus* abundance in our in-house 16s rRNA gene sequencing dataset across different stages of gastric tumorigenesis. Compared with *S. anginosus* levels in superficial gastritis, *S. anginosus* is elevated in atrophic gastritis and IM and reached the highest abundance in patients with GC (Figures 1A and S1A). In this cohort, *S. anginosus*-positive subjects have an increased prevalence of atrophy gastritis (AG)/IM and GC (Table S1). A follow-up study comparing the gastric microbiome 1 year after *H. pylori* eradication also identified that *S. anginosus* was associated with persistent gastric inflammation (Figure S1B).[9] Increased abundance of *S. anginosus* in GC compared with superficial gastritis ($p = 0.024$) was also observed in an independent European cohort (Figure S1C).[10] Moreover, *S. anginosus* was enriched in GC tumors compared with paired adjacent normal tissues ($p = 0.003$) (Figure S1C).[11] These studies suggest the potential role of *S. anginosus* in GC progression. To explore the pathogenic role of *S. anginosus* in mouse stomach, we gavaged *S. anginosus* in conventional mice once every 3 days for 2 weeks (Figure 1B). This gavage interval ensured continuous colonization of *S. anginosus* in the gastric mucosa (Figure S1D). Brain heart infusion (BHI) broth was given as a negative control, while *H. pylori SS1* was gavaged to mice as a positive control. At 2 weeks post-infection, we observed the colonization of *S. anginosus* in the basal area of gastric mucosa by fluorescence *in situ* hybridization (FISH) (Figure 1C). *S. anginosus* colonization in the stomach was confirmed by PCR detection of bacterial DNA (Figure S1E) and culture of live bacteria from fresh gastric tissues (Figure S1F). We observed acute inflammation in *S. anginosus*-infected mice, evidenced by neutrophil infiltration in the submucosa given by a pathologist under H&E staining (Figure 1D), and 26% (6 of 23) of *S. anginosus*-infected mice showed mild to moderate inflammation (Figure 1E) according to an established histological scoring scheme.[12] As a positive control, *H. pylori* caused mild to moderate inflammation in 44.5% (8 of 18) of mice (Figure 1E). In keeping with *S. anginosus*-induced acute inflammation, the expression of pro-inflammatory chemokines was upregulated in *S. anginosus*-gavaged mice as determined by the mouse inflammatory response and autoimmune PCR array on gastric tissues (Figure 1F). The induction of pro-inflammatory chemokines including *Ccl20* ($p = 0.03$) and *Ccl8* ($p = 0.005$) was validated by qPCR, and both were upregulated in *S. anginosus*-infected mice compared with BHI control mice (Figure 1G; Table S2). These results indicated that *S. anginosus* infection in mice induced acute inflammation in the stomach concomitant with significant elevation of pro-inflammatory chemokines.

### *S. anginosus* induces chronic gastritis in mice following 3 months of infection

To determine the long-term effect of *S. anginosus* infection in stomach, we extended our infection model to 3, 6, 9, and 12 months (Figure 2A). *S. anginosus* infection had no effect on body weight (Figure S2A), food intake (Figure S2B), or liver-to-body weight ratio (Figure S2C). Markers of liver function (alanine transaminase [ALT] and aspartate aminotransferase [AST]) (Figure S2D) and renal function (creatinine < 0.4 mg/dL) were normal in *S. anginosus*-infected mice. *S. anginosus* did not cause inflammation in the colon (Figures S2E–S2G). On the other hand, persistent *S. anginosus* infection in the basal area of gastric mucosa with expansion to the mucosal layer was evidenced by FISH in both the antrum and corpus (Figures 2B, S2H, and S2I), and the presence of live *S. anginosus* was confirmed by bacterial culture from fresh stomach tissues (Figures S2J and S2K; Table S3). Along with *S. anginosus* infection, we observed chronic inflammation as evidenced by the continuous infiltration of neutrophils and lymphocyte foci formation beneath the gastric mucosa starting from 3 months post-infection, which persisted to 6, 9, and 12 months (Figure 2C). Gastric inflammation score was significantly increased in *S. anginosus*-infected mice at 9 months post-infection compared with that in BHI control mice ($p = 0.006$), which was intensified at 12 months post-infection ($p < 0.0001$) (Figure 2D). In particular, *S. anginosus* infection elicited equivalent levels of inflammation to *H. pylori* infection, especially at later time points. Moreover, co-infection of *H. pylori* and *S. anginosus* increased gastric inflammation compared with *S. anginosus* or *H. pylori* infection alone at 3 months post-infection (Figures S3A–S3C). In agreement with this, analysis of our in-house dataset (Figure 1A) revealed that subjects co-infected with *S. anginosus* and *H. pylori* had higher relative risks of atrophic gastritis and subsequent disease progression to IM and GC compared with *H. pylori* infection alone (Table S4). Together, these results suggested that long-term *S. anginosus* infection caused intensive chronic gastritis that is comparable with *H. pylori* infection, and these two pathogens might act collaboratively to promote gastric inflammation.

### *S. anginosus* provokes spontaneous gastric atrophy, metaplasia, and dysplasia in mice following 9 months of infection

Gastric tumorigenesis proceeds along the precancerous lesion of atrophy-metaplasia-dysplasia sequence, with gastritis being a major risk factor.[13] Given that *S. anginosus* caused chronic gastritis, we asked if long-term infection could trigger precancerous lesions in the gastric mucosa. At 9 months, *S. anginosus* infection caused mild parietal cell atrophy, which progressed to moderate to severe atrophy at 12 months ($p = 0.01$) (Figure 3A). Moreover, mucinous metaplasia was detected in *S. anginosus*-infected mice at 12 months post-infection (Figure 3B). Importantly, *S. anginosus*-infected mice formed low-grade dysplasia at 12 months post-infection (Figures 3C and 3D). FISH analysis of mouse gastric tissues demonstrated that *S. anginosus* was enriched in metaplasia/dysplasia regions compared with non-metaplasia regions (Figure S3D). *H. pylori*, as positive control, more rapidly induced gastric atrophy; however, the number of mucinous metaplasia was lower than that induced by *S. anginosus* at 12 months, and no dysplasia was identified (Figure 3A, 3B, and 3E). Consistent with the induction of gastric atrophy, *S. anginosus* elevated gastric pH after 9 and 12 months ($p < 0.05$) of infection compared with the BHI control group (Figures S3E and S3F).

To confirm the mucinous metaplasia, we performed histological staining with Alcian blue, a dye frequently used to indicate goblet cells in stomach for the diagnosis of IM.[14] As shown in Figure 3E,

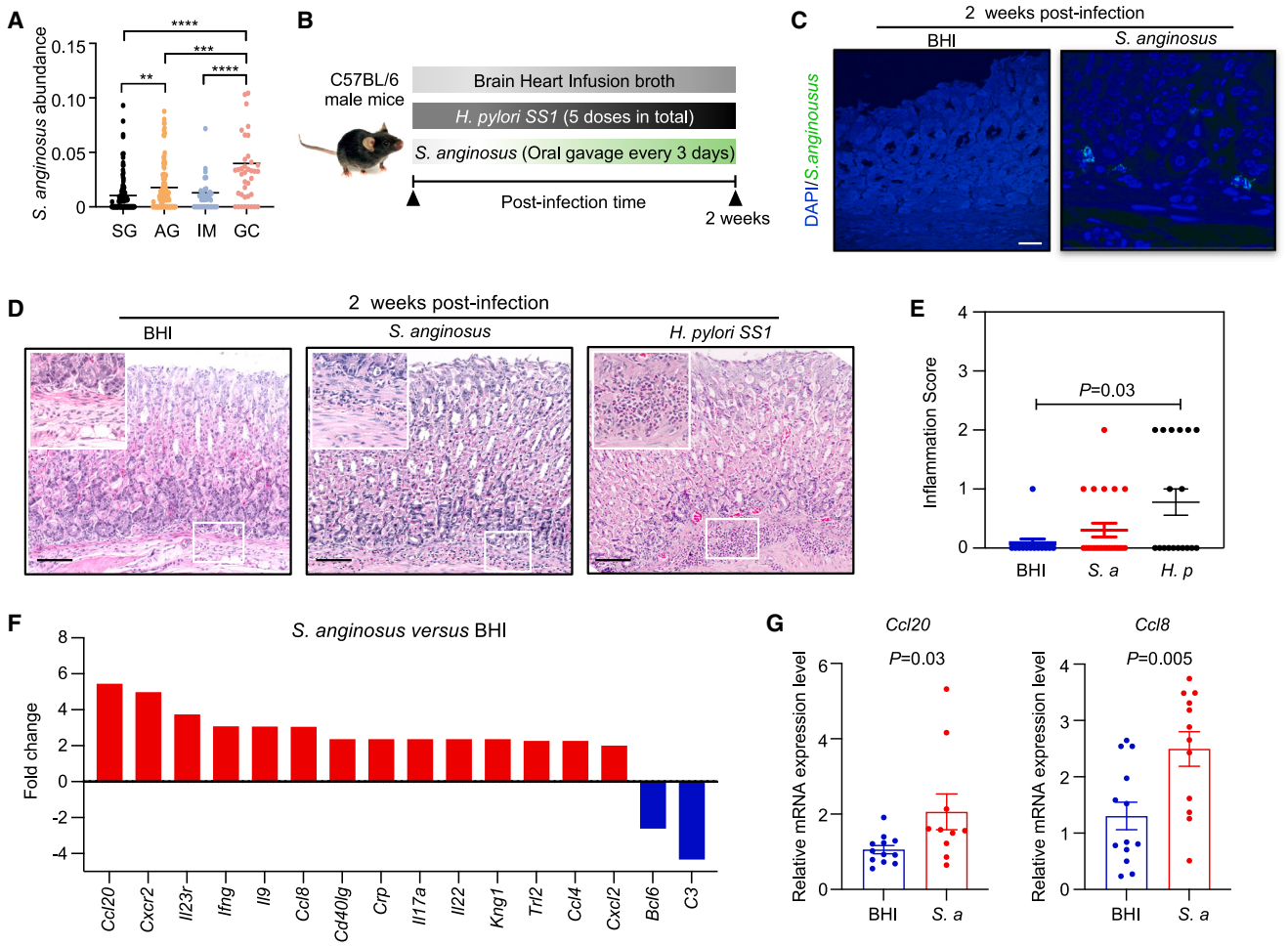


**Figure 1. *Streptococcus anginosus* colonizes gastric mucosa and promotes acute inflammation**

(A) Abundance of *Streptococcus anginosus* (*S. anginosus*) in gastric biopsies from superficial gastritis (SG, N = 110), atrophy gastritis (AG, N = 117), intestinal metaplasia (IM, N = 45), and gastric cancer (GC, N = 39) patients. *p < 0.05, ** p < 0.01, ***p < 0.001, **** p < 0.0001.

(B) C57BL/6 male mice were orally gavaged with *Streptococcus anginosus* (*S. anginosus*, n = 23), *Helicobacter pylori SS1* (*H. pylori*, n = 18), or brain heart infusion broth (BHI, n = 13) for 2 weeks.

(C) Representative fluorescence *in situ* hybridization (FISH) images of gastric tissue sections from mice gavaged with *S. anginosus* or BHI at 2 weeks post-infection (blue: nuclear, green: *S. anginosus* probe); scale bars, 20 μm.

(D) Representative H&E images of the stomach from mice infected with *S. anginosus*, *H. pylori SS1*, or BHI broth at 2 weeks post-infection; scale bars, 100 μm.

(E) Gastric inflammation scores of the different groups. Score 0, no inflammation; score 1, mild; score 2, moderate; score 3, severe; score 4, critical.

(F) Mouse inflammatory response and autoimmunity PCR array revealed 14 upregulated pro-inflammatory genes in *S. anginosus*-infected mice at 2 weeks post-infection.

(G) Gastric *Ccl8* and *Ccl20* mRNA levels were upregulated by *S. anginosus* infection at 2 weeks post-infection. Data were shown as mean ± SEM. Each spot represents one subject. Two-tailed Wilcoxon ranked sum test (A), Kruskal-Wallis test (E), or Student's t test (G) was used to examine the statistical significance among groups.

See also Figure S1 and Tables S1, S2, and S4.

Alcian blue-positive cells were found in gastric mucosa in *S. anginosus*-infected mice, but not in BHI control mice at 12 months. We also performed immunofluorescence staining of metaplastic marker *Griffonia simplicifolia* lectin II (GSII) (Figure 3F). Consistent with the metaplastic changes under H&E staining, *S. anginosus* infection increased GSII-positive cells within gastric glands at 12 months post-infection. Moreover, *S. anginosus* induced cell proliferation in gastric mucosa as determined by Ki-67 (Figure 3G) and proliferating cell nuclear antigen (PCNA) staining, respectively, (Figure 3H) at 6 and 12 months post-infection. Notably, infection with another GC-enriched oral pathogen, *Parvimonas micra* (Figure S3G), only induced mild to moderate inflammation in the mouse stomach after 12 months, with no sign of gastric atrophy or metaplasia (Figures S3H and S3I), inferring that the induction of gastric tumorigenesis is specific to *S. anginosus*. Collectively, these results support the notion that *S. anginosus* infection specifically triggered a series of precancerous changes in gastric mucosa, manifested by progressive parietal cell atrophy, mucinous metaplasia, and dysplasia, accompanied by increased cell proliferation.

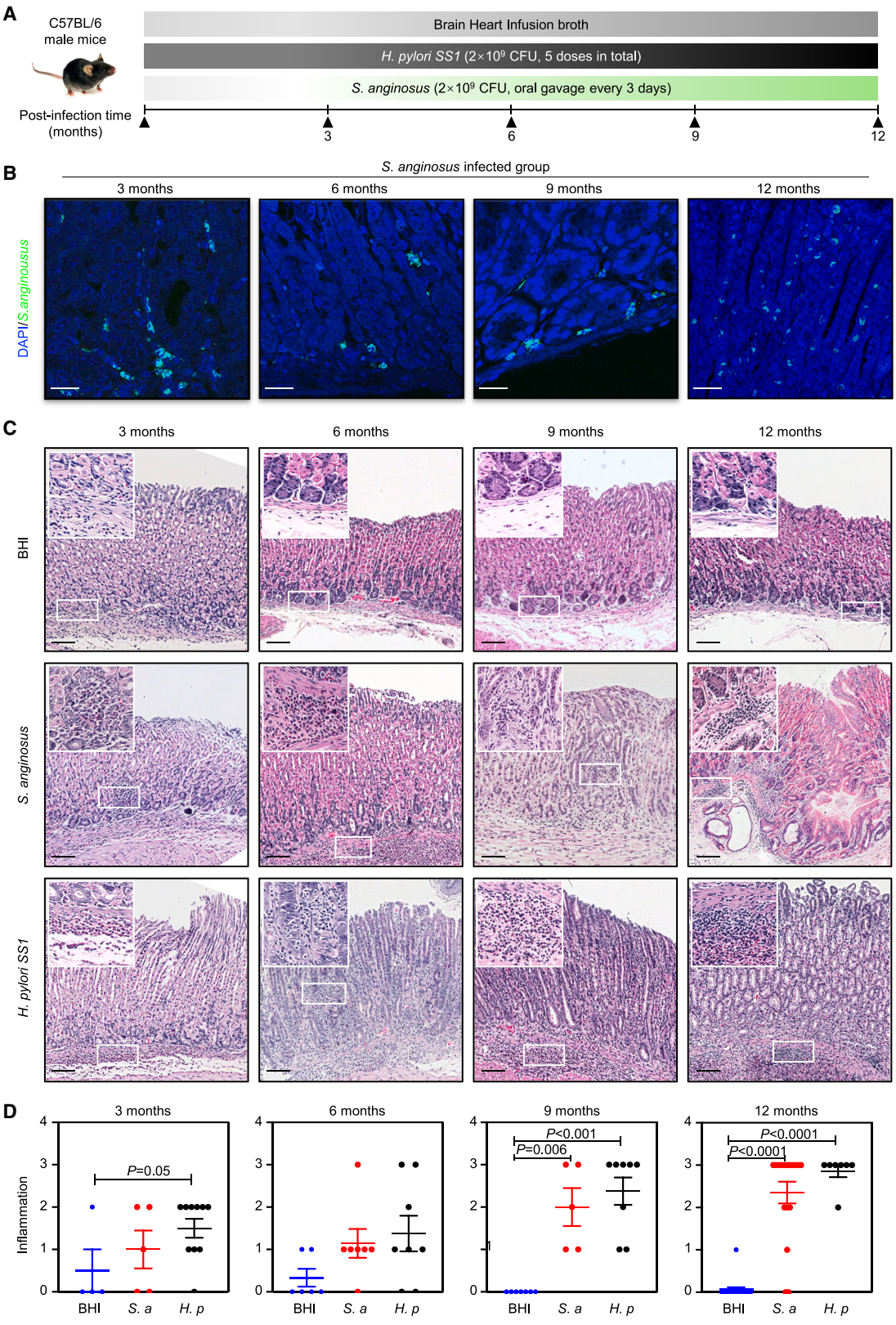


(legend on next page)

### *S. anginosus* impairs gastric barrier function and gastric microbiome homeostasis in mice

The disruption of gastric barrier function is an important hallmark of neoplastic transformation.[15] Claudin18 (CLDN18) is a tight junctional protein specifically expressed in the stomach.[16,17] We thus examined the expression of CLDN18 together with junctional markers Occludin (OCLN) and Zonula occludens (ZO-1) by western blot. As shown in Figure 3I, CLDN18 ($p < 0.001$), OCLN ($p = 0.018$), and ZO-1 ($p = 0.006$) proteins were significantly decreased in *S. anginosus*-infected mice compared with BHI control mice. Consistently, CLDN18 was disrupted at the neck region of the corpus and the base of the antrum after 3 months of *S. anginosus* infection as indicated by immunofluorescence staining (Figure 3J). Consequently, the loss of CLDN18 was apparent along the entire length of gastric glands in corpus or antrum at 9 and 12 months post-infection. Furthermore, *S. anginosus* infection functionally impacts gastric barrier function, as evidenced by its capacity to increase transepithelial fluorescein isothiocyanate (FITC) permeability in MKN28 and NCI-N87 monolayer cells (Figure S3J). These results implied the disruption of gastric barrier function by *S. anginosus* infection.

To unravel alterations in the gastric microbiome after *S. anginosus* or *H. pylori* infection, we performed 16s rRNA sequencing of gastric mucosa from *S. anginosus*- and *H. pylori*-infected mice at acute (2 weeks), chronic (3 and 6 months), and precancerous (9 and 12 months) stages. Compared with the *S. anginosus* infection at acute and chronic stages, the infection at precancerous stage enriched *Sutterella*; *Parabacteroides*; and oral commensals *Bacteroides*, *Prevotella*, and *Aggregatibacter*, together with the depletion of probiotics such as *Bifidobacterium pseudolongum* and *Lactobacillus* (Figure S3K). *Prevotella* and *Aggregatibacter* were reported to be increased in the oral cavity of patients with GC compared with healthy subjects,[18] while *Aggregatibacter* was also enriched in the gastric microbiota of GC compared with superficial gastritis.[19] Network analysis further highlighted a negative correlation between *B. pseudolongum* and *S. anginosus* at precancerous stage (Figure S3L; Table S5). This indicates that *S. anginosus* infection might increase oral commensals and reduce probiotics in the stomach that fuel its pro-inflammatory and pro-tumorigenic effects. Consistent with our finding, oral microbial community including *Streptococcus* is associated with pseudoantralized IM inflammatory microenvironment.[20] Meanwhile, *H. pylori* at precancerous stage enriched *Lactobacillus*, *Streptococcus*, *Eubacterium*, and *Prevotella*, together with the depletion of *B. pseudolongum* (Figures S3M and S3N; Table S5).

### *S. anginosus* induces spontaneous mucinous metaplasia in germ-free mice

We then asked whether *S. anginosus* could promote gastric tumorigenesis as a single bacterium. To this end, *S. anginosus* was inoculated into germ-free mice for 9 months (Figure 4A). The successful colonization of *S. anginosus* in gastric mucosa of germ-free mice was confirmed by FISH, PCR, and qPCR, and bacterial culture of fresh gastric tissues indicated the presence of live *S. anginosus* (Figures 4B–4E). Histological assessment of BHI control mice showed no abnormalities, whereas *S. anginosus*-infected mice harbored mucinous metaplasia (3 of 8; $p = 0.035$) at 9 months post-infection (Figures 4F and 4G). Consistently, *S. anginosus* promoted cell proliferation, as evidenced by increased Ki-67-positive cells ($p = 0.007$) (Figures 4H and 4I). CLDN18 and OCLN protein expressions were significantly downregulated by *S. anginosus*, implying that *S. anginosus* disrupted gastric tight junction in germ-free mice (Figure 4J). Collectively, our results from germ-free mice confirmed the direct pathogenic effect of *S. anginosus* in driving gastric tumorigenesis.

### *S. anginosus* promotes the growth of YTN16 allografts *in vivo*

To investigate if *S. anginosus* promotes GC progression, we established a GC allograft model by the subcutaneous implantation of murine GC YTN16 cells,[21] a model of microsatellite instability (MSI) GC (Table S6), to C57BL/6 mice, followed by intratumoral *S. anginosus* injections (Figure 5A). *S. anginosus* significantly promoted allograft growth ($p < 0.01$) (Figure 5B). At the end point, *S. anginosus*-injected tumors showed significantly increased tumor size (Figure 5C) and tumor weight (Figure 5D) compared with control mice injected with phosphate-buffered saline (PBS). Consistently, *S. anginosus* increased cell proliferation and suppressed apoptosis, as indicated by increased Ki-67-positive cells (Figure 5E) and reduced terminal deoxynucleotidyl transferase (TdT)-mediated dUTP nick end labeling (TUNEL)-positive bodies (Figure 5F), respectively, in YTN16 allografts.

We also established an orthotropic GC allografts mouse model by injecting YTN16 cells into the gastric serosa layer.[22] Mice were gavaged with *S. anginosus* once every 3 days from the second week for 6 weeks. At the end point, *S. anginosus*-infected mice showed significantly increased tumor weight ($p = 0.03$) and tumor-to-stomach weight ratio ($p = 0.003$) (Figures 5G–5I) compared with control mice gavaged with BHI broth. To evaluate the effect of *S. anginosus* on GC cell states, we further performed single-cell RNA sequencing (scRNA-seq) of *S. anginosus*-infected orthotopic YTN16 GC tumors

**Figure 2. *Streptococcus anginosus* promotes chronic gastritis in mice**

(A) C57BL/6 male mice were orally gavaged with *S. anginosus* (n = 5 for 3 months, n = 7 for 6 months, n = 5 for 9 months, n = 17 for 12 months), *H. pylori SS1* (n = 10 for 3 months, n = 8 for 6 months, n = 8 for 9 months, n = 8 for 12 months), or BHI broth (n = 4 for 3 months, n = 6 for 6 months, n = 7 for 9 months, n = 17 for 12 months) for 3, 6, 9, and 12 months.

(B) Representative FISH images of gastric tissue sections from *S. anginosus*-infected mice (3, 6, 9, and 12 months post-infection) (blue: nuclear, green: *S. anginosus* probe); scale bars, 20 μm.

(C) Representative H&E images of stomach of mice gavaged with BHI, *H. pylori SS1*, and *S. anginosus* (3, 6, 9, and 12 months post-infection); scale bars, 100 μm.

(D) Corresponding histological scores were shown by inflammation and parietal cell atrophy. Data were shown as mean ± SEM. Each spot represents one subject. Kruskal-Wallis test (D) was used to determine the statistical significance among groups.

See also Figure S2.

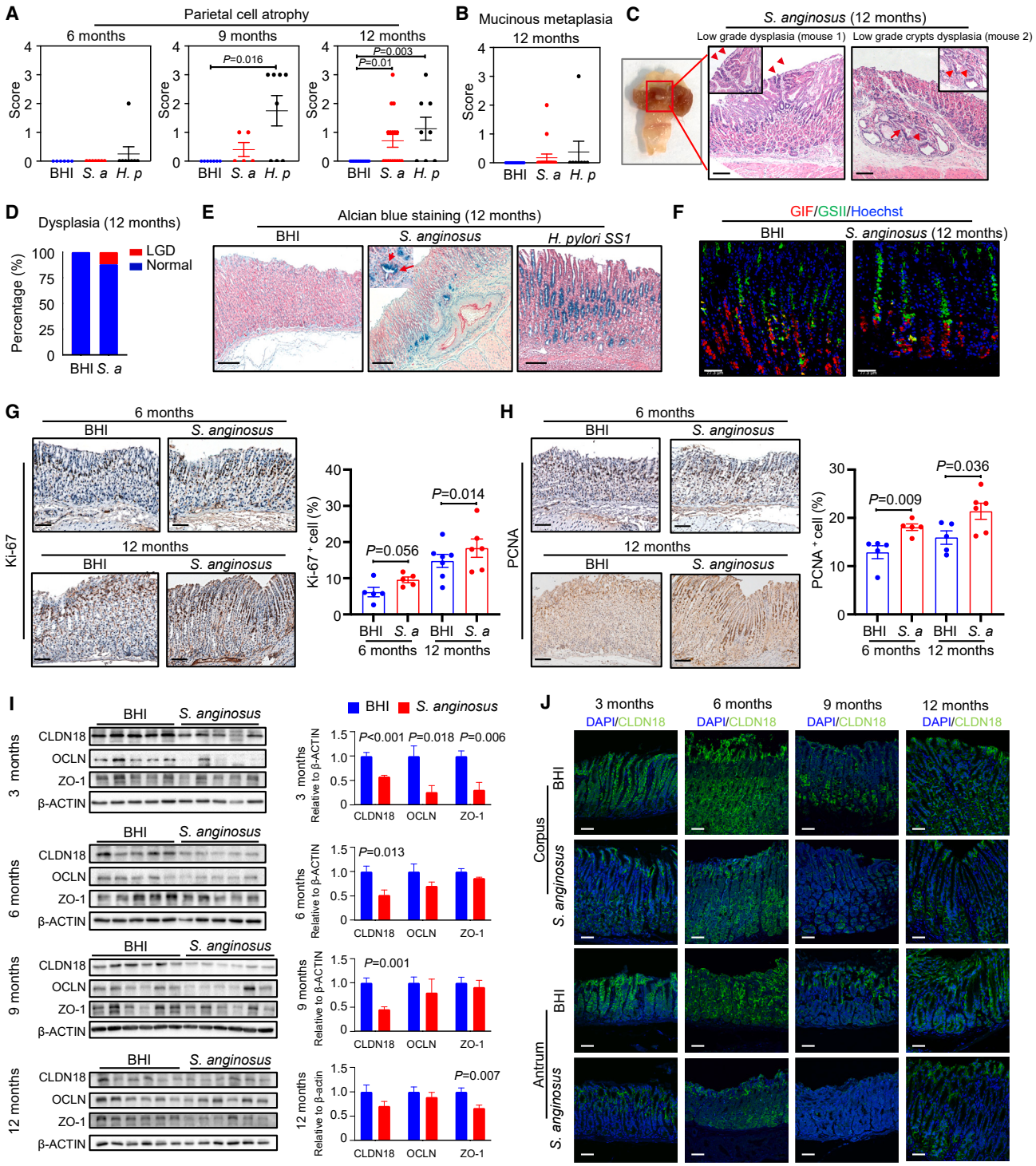


**Figure 3. *Streptococcus anginosus* induces gastric atrophy, metaplasia, and dysplasia along with impaired gastric barrier function in mice**

(A and B) Histological analysis of the stomach of mice gavaged with BHI, *H. pylori SS1*, and *S. anginosus* (3, 6, 9, and 12 months post-infection) revealed the presence of parietal cell atrophy and mucinous metaplasia.

(C) *In situ* image of the stomach from *S. anginosus*-infected mice at 12 months post-infection and corresponding images of H&E staining displayed low-grade dysplasia; scale bars, 100 μm.

(D) The incidence of gastric low-grade dysplasia (LGD) in *S. anginosus*-infected mice at 12 months post-infection.

*(legend continued on next page)*

(Figure S4A). Unsupervised clustering of malignant cells identified 7 cell subclusters, suggesting significant heterogenicity in YTN16 tumors (Figure S4B). Compared with the control, *S. anginosus* reduced the proportion of differentiated GC cells, with a corresponding increase in clusters with activated inflammatory response, epithelial–mesenchymal transition (EMT), and angiogenesis pathways (Figures S4C and 4D; Table S7). Next, we mapped tumor-infiltrating immune cells based on scRNA-seq datasets. *S. anginosus*-infected YTN16 tumors were enriched in pro-inflammatory Th17, immunosuppressive tumor-associated macrophages (Angio-TAM and LA-TAM), polymorphonuclear myeloid-derived suppressor cells (PMN-MDSCs), and exhausted $CD8^+$ T cells (Figures S4E–S4H), inferring that *S. anginosus* promotes a pro-inflammatory and an immunosuppressive tumor microenvironment. These results suggested that *S. anginosus*-YTN16 interaction altered cell states and reshaped the tumor microenvironment in GC to promote tumorigenesis. Collectively, these data indicated that *S. anginosus* promoted the growth of GC allografts *in vivo*.

### *S. anginosus* accelerates gastric tumorigenesis in mice

To clarify the role of *S. anginosus* in gastric tumorigenesis, we established an N-methyl-N-nitrosourea (MNU)-induced GC mouse model (Figure 5J). Gastric lesions were observed in the antrum after 9 months of MNU treatment (Figures 5K and S4I). *S. anginosus*-infected mice showed significantly increased tumor incidence (10 of 11, $p = 0.003$) compared with control mice (4 of 13) and *H. pylori*-infected mice (12 of 18, $p < 0.05$) (Figures 5K and S4J). Consistently, both tumor number ($p = 0.006$) and tumor size ($p < 0.05$) were significantly higher in *S. anginosus*-infected mice compared with control mice treated with MNU only (Figure 5L). Histological examination showed that 36.4% of *S. anginosus*-infected mice had high-grade dysplasia (HGD), which was higher than that observed in mice treated with MNU alone (15.4%) (Figure 5M) and was comparable with that in *H. pylori*-infected mice (22.2% HGD and 5.6% adenocarcinoma) (Figure S4K). Accordingly, *S. anginosus* induced higher cell proliferation in mice compared with MNU-treated control mice by Ki-67 staining ($p < 0.05$) (Figure 5N). These findings collectively inferred that *S. anginosus* accelerates gastric tumorigenesis in mice induced by MNU.

### *S. anginosus* surface protein TMPC binds to ANXA2 receptor on gastric epithelial cells for *S. anginosus* colonization

Since we identified that *S. anginosus* could colonize in the gastric mucosa of mice, we investigated the adhesion properties of this bacterium. Bacterial attachment and invasion assays, respectively, showed that *S. anginosus* (multiplicity of infection [MOI] = 50) could attach onto and invade into AGS and Ges-1 cells (Figure 6A). We then performed scanning electron microscopy (SEM) to visualize the attachment of *S. anginosus* to gastric epithelial cells. As shown in Figure 6B, *S. anginosus* (<1 μm, coccoid-like shape) is attached onto the surface of AGS and Ges-1 cells with a clear pathogen-host interface. This indicates that *S. anginosus* may exert its oncogenic effect through direct interactions with gastric epithelial cells.

To decipher the underlying mechanism by which *S. anginosus* attaches onto and invades into gastric epithelial cells, we sought to identify bacterial adhesins that are capable of binding host receptors. Biotin pull-down assay was used to probe potential interactions between *S. anginosus* adhesins and Ges-1 membrane proteins (Figure 6C). Mass spectrometry identified three *S. anginosus* proteins of which only TMPC is a surface protein (Table S8). TMPC is a lipoprotein belonging to ATP-binding cassette (ABC)-like transporter family, and it functions as a transporter for purine nucleotides.[23] Homology alignment of *S. anginosus* TMPC revealed that it shared high homology with bacteria in the *Streptococcus* genus, many of which were enriched in GC biopsies (Figure S5A). *Tmpc* gene is constitutively expressed in *S. anginosus*, and its expression level is unaffected by contact with gastric epithelial cells (Figure S5B). We then looked for the binding receptor of TMPC on gastric epithelial cells. We expressed glutathione S-transferase (GST)-tagged TMPC recombinant protein (GST-TMPC) in *E. coli* and performed GST pull-down with Ges-1 membrane proteins (Figure 6D). Over 10 candidate bands were identified in Ges-1 and AGS cells (Figures 6E and S5C). Overlap of the candidate proteins from these cell lines unraveled ANXA2 as a common receptor for TMPC (Table S8). Co-immunoprecipitation (co-IP) assays consistently showed pull-down of ANXA2 by GST-TMPC in Ges-1 and AGS cells (Figure 6F), which was validated by reciprocal co-IP using anti-ANXA2 (Figure 6G). Moreover, direct interaction between TMPC and ANXA2 was confirmed by co-IP assays with recombinant ANXA2 and recombinant GST-TMPC (Figure 6H) and by microscale thermophoresis (MST) (Figure 6I). MST is a revolutionary technique to analyze biomolecular interactions,[24] which demonstrated the binding of ANXA2 to TMPC with an apparent dissociation constant ($K_d$) of 57.4 μM (Figure 6I).

The functional role of TMPC- ANXA2 in mediating the colonization of *S. anginosus* in gastric epithelial cells was validated by depleting *ANXA2* in Ges-1 and AGS cells by small guide RNA (sgRNA) (Figure 6J). *ANXA2* knockout inhibited *S. anginosus*

(E) Alcian blue staining, which is mucinous metaplasia marker, revealed acidic mucin-containing glands in the corpus of stomach from *S. anginosus*- and *H. pylori*-infected mice at 12 months post-infection; scale bars, 100 μm.
(F) Aberrant chief cell marker (gastric intrinsic factor [GIF]) and enhanced expression of mucus neck cell marker (GSII) were observed in *S. anginosus*-infected mice at 12 months post-infection; scale bars, 50 μm.
(G and H) *S. anginosus*-infected mice showed a higher expression level of cell proliferation marker Ki-67 (G) and proliferating cell nuclear antigen (PCNA) (H) in the stomach at 6 and 12 months post-infection; scale bars, 100 μm.
(I) Gastric tight junction markers Claudin18 (CLDN18), Occludin (OCLN), and Zonula occludens (ZO-1) were downregulated in *S. anginosus*-infected mice compared with BHI broth control at 3, 6, 9, and 12 months post-infection.
(J) Representative immunofluorescence images of CLDN18 staining in the gastric mucosa; scale bars, 50 μm. Data were shown as mean ± SEM. Each spot represents one subject. The Kruskal-Wallis test (A and B) or Student's t test (G–I) was used to examine the statistical significance among groups.
See also Figure S3.

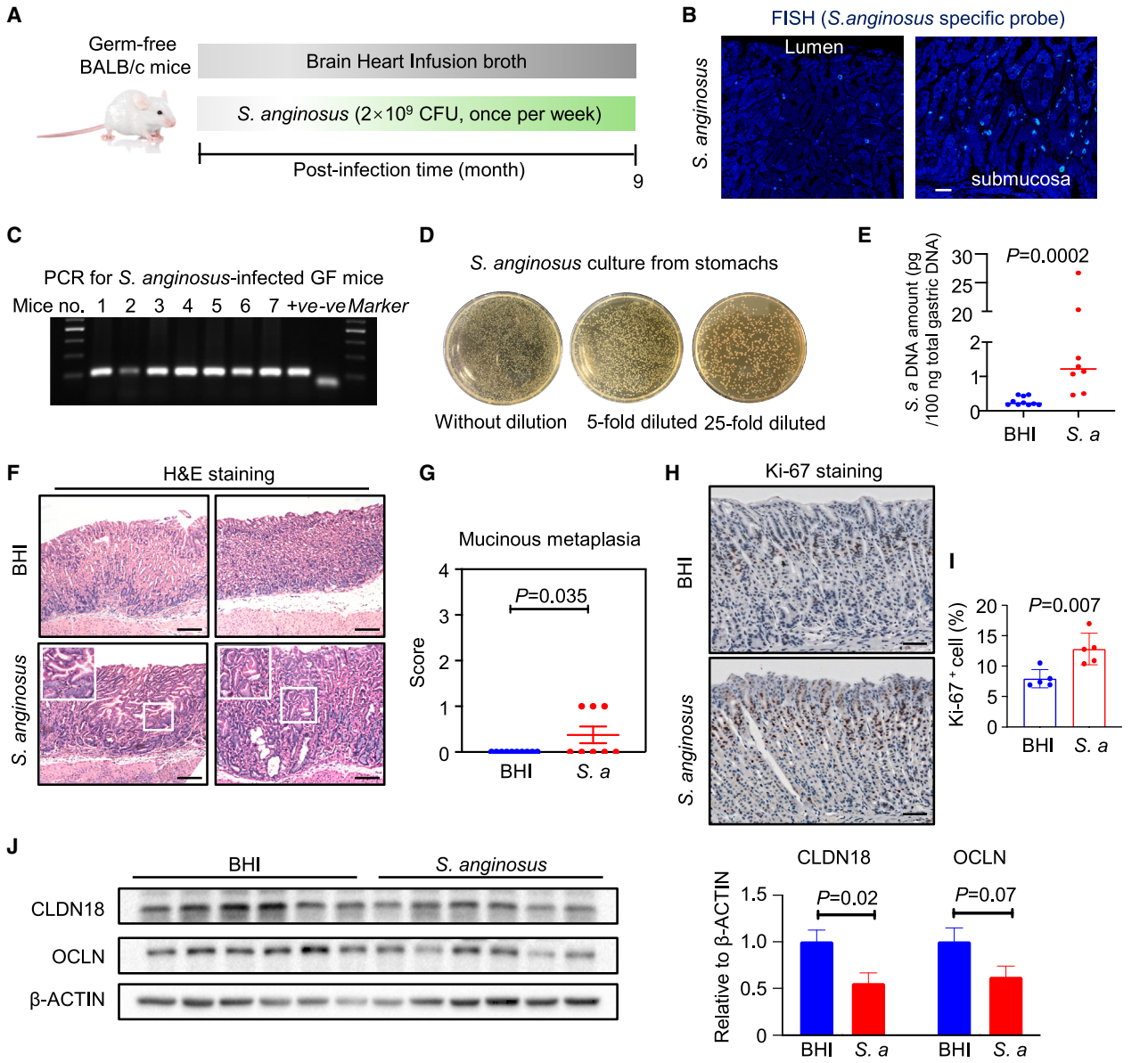


**Figure 4. *Streptococcus anginosus* promotes mucinous metaplasia in germ-free mice**

(A) Germ-free BALB/c mice were gavaged with *S. anginosus* (n = 8) or BHI broth (n = 10) once per week for 9 months.

(B–E) *S. anginosus* colonization and bacteria loads were confirmed by FISH (scale bars, 20 μm) (B), PCR (C), bacterial culture of fresh gastric mucosa tissue (D), and qPCR (E) from *S. anginosus*-infected germ-free mice.

(F) Representative H&E image of gastric mucosa from germ-free mice administrated with *S. anginosus* or BHI broth; scale bars, 200 μm.

(G) Mucinous metaplasia score was shown.

(H and I) Cell proliferation marker Ki-67 was upregulated in *S. anginosus*-infected germ-free mice; scale bars, 50 μm.

(J) Tight junction markers CLDN18 and OCLN were downregulated in the stomach of *S. anginosus*-infected germ-free mice. Data were shown as mean ± SEM. Each spot represents one subject. Mann-Whitney U test (E) and Student's t test (G, I, and J) were used to examine the statistical significance among groups.

attachment and invasion compared with small guide negative control (sgNC) cells (Figures 6K and S5D). To determine the functional importance of TMPC in *S. anginosus*-driven gastric tumorigenesis, we utilized insertional inactivation (Figure 6L) to generate an *S. anginosus*Δ*Tmpc* mutant strain (Figures 6M and S5E) deficient in TMPC protein expression (Figure 6N). Compared with wild-type *S. anginosus*, *S. anginosus*Δ*Tmpc* showed markedly impaired cell adhesion and invasion ability *in vitro* (Figures 6O and S5F) and failed to induce the growth of YTN16 allografts *in vivo* (Figures 6P and 6Q). Together, these findings confirmed that TMPC mediates *S. anginosus* colonization of gastric epithelial cells through its surface protein TMPC binding to ANXA2 receptor on gastric epithelial cells and is functionally essential for tumorigenesis.

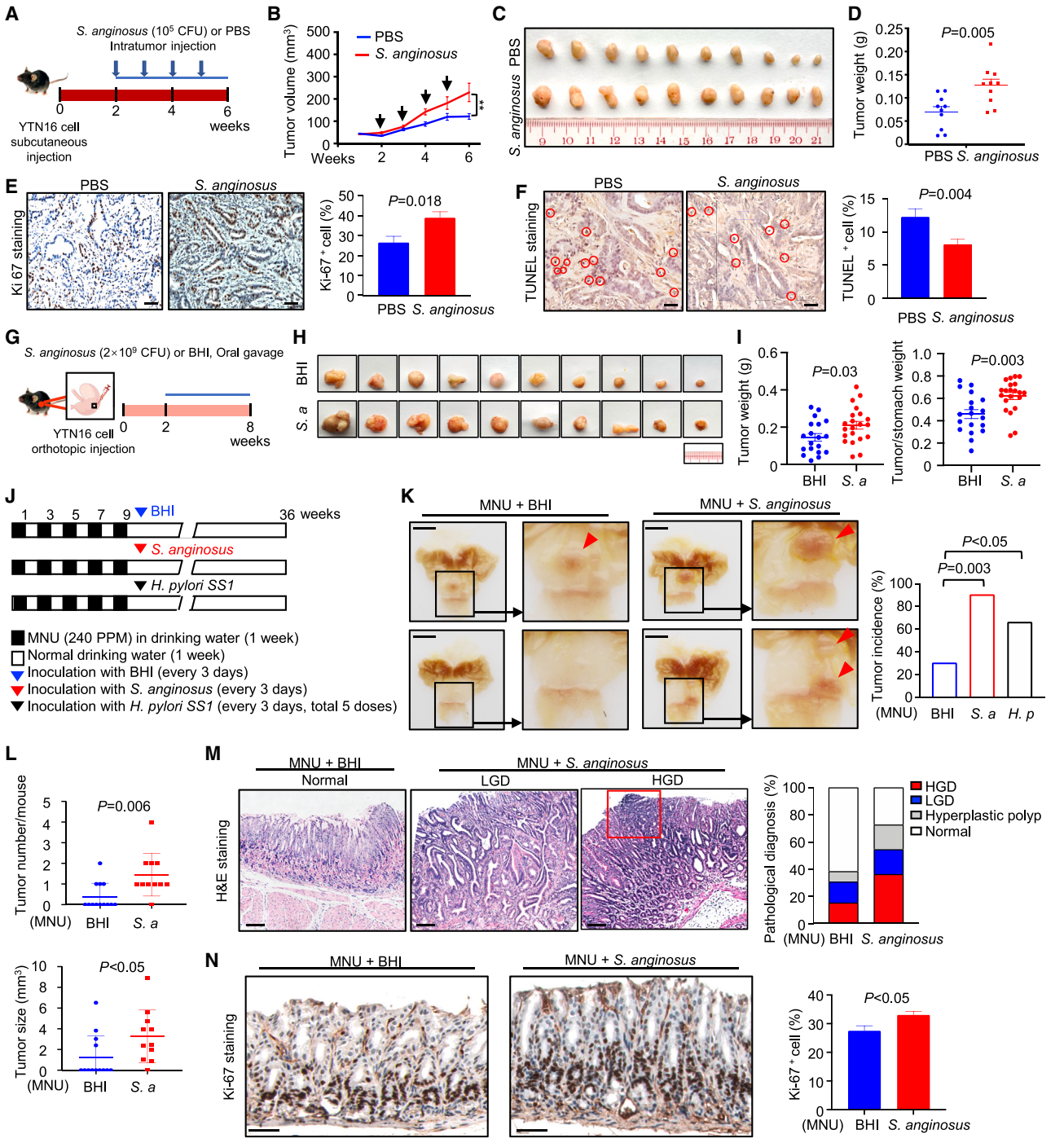


**Figure 5. *Streptococcus anginosus* accelerates gastric cancer development in mice**

(A) C57BL/6 mice were intratumorally injected with *S. anginosus* ($10^5$ colony-forming unit [CFU], n = 10) or PBS (n = 10) once per 5 days in YTN16 allograft model of gastric carcinoma.

(B–D) Tumor growth curve, (C) images of tumors, and (D) tumor weight from *S. anginosus*- or PBS-injected YTN16 allografts. Tumor weight was shown as mean ± SEM. **p < 0.01.

(E) Ki-67 staining showed increased cell proliferation rate in tumors from *S. anginosus*-injected mice compared with PBS control mice; scale bars, 50 μm.

(F) Terminal deoxynucleotidyl transferase (TdT)-mediated dUTP nick end labeling (TUNEL) staining revealed decreased apoptotic cells in tumors from *S. anginosus*-infected mice; scale bars, 50 μm.

(G) C57BL/6 mice were orally gavaged with *S. anginosus* ($2 \times 10^9$ CFU, n = 21) or BHI (n = 19) once per 3 days in YTN16 orthotropic gastric cancer model.

*(legend continued on next page)*

### *S. anginosus* activates MAPK signaling pathway through TMPC-ANXA2 interaction

To investigate the downstream signaling mechanisms involved in *S. anginosus*-induced gastric carcinogenesis, we performed RNA-seq of gastric tissues from *S. anginosus*-infected conventional mice (12 months) and of those from control mice. Volcano plots showed that 1,727 genes were upregulated, and 1,020 genes were downregulated in *S. anginosus*-infected mice (Figures 7A and S6A). Pathway enrichment analysis identified that several oncogenic pathways including Ras, MAPK, and phosphatidylinositol 3-kinase (PI3K)-AKT were upregulated in *S. anginosus*-infected mice (Figure 7B). Enrichment score showed that MAPK signaling was significantly activated by *S. anginosus* infection (Figure 7C). Indeed, protein expressions of p-ERK1/2, p-JNK, and p-AKT were markedly increased in *S. anginosus*-infected mice as shown by western blot (Figure 7D), concomitant with the induction of downstream Cyclin D1 (Figure 7D). We validated our observations in MNU GC mice (9 months). Similarly, *S. anginosus* significantly increased the protein expressions of p-ERK1/2 ($p = 0.006$); p-AKT ($p = 0.006$); p-c-Jun ($p = 0.002$), concomitant with downstream Cyclin D1 ($p = 0.048$); and c-Myc ($p = 0.018$) (Figure 7E). *S. anginosus* also induced p-ERK1/2 and p-JNK in the stomach of germ-free mice at 9 months post-infection (Figure S6B). Moreover, co-culture of *S. anginosus* with Ges-1 and AGS cells rapidly increased p-ERK1/2, p-AKT, and p-JNK protein expressions (Figure 7F). Consistently, *S. anginosus* also attached and invaded KRAS wild-type GC cell lines, MKN28 and NCI-N87 (Figure S6C), and activated MAPK signaling (Figure S6D). The activation of MAPK signaling by *S. anginosus* critically depends on the TMPC-ANXA2 interaction. Knockout of *ANXA2* in Ges-1 and AGS cells abolished the induction of p-ERK1/2, p-AKT, and p-JNK by *S. anginosus* (Figure 7G). Recombinant TMPC protein also induced p-ERK1/2, p-AKT, and p-JNK in AGS and NCI-N87 cells (Figure S6E). In addition, the deletion of TMPC abrogated the induction of p-ERK1/2 and p-JNK by *S. anginosus* in YTN16 allografts *in vivo* (Figure 7H). Our results collectively indicated that *S. anginosus* promotes MAPK signaling through the TMPC-ANXA2 interaction, which in turn contributes to its pro-tumorigenic effect in the gastric epithelium.

## DISCUSSION

*H. pylori* has long been considered the causative agent in gastric tumorigenesis; however, its dominance in the gastric mucosa is largely diminished as the disease progresses to atrophy, metaplasia, and GC stages. Intrigued by this observation, we sought to establish a role of non-*H. pylori* microbiome in GC. Our metagenomic profiling of gastric mucosal samples across different stages of GC revealed that *S. anginosus* is a potential pathogen enriched in GC.[5,9] Here, we demonstrate the causality of *S. anginosus* in gastric tumorigenesis and establish a mechanism through which *S. anginosus* communicates with gastric epithelial cells to drive oncogenesis.

*S. anginosus* readily colonizes the murine stomach and initiates an acute inflammation response with upregulated pro-inflammatory cytokines including Ccl20 and Ccl8, followed by a chronic phase with intensive and persistent gastritis. Chronic inflammation is an environmental trigger for gastric tumorigenesis.[25] Consistently, we found that long-term *S. anginosus* infection caused progressive gastric pathologies, including parietal cell atrophy, mucinous metaplasia, and dysplasia. *S. anginosus*-induced metaplastic transformation, as evidenced by histology and confirmed by increased Alcian blue-positive cells and the GSII-positive mucous neck cells, together with reduced gastric intrinsic factor (GIF)-positive chief cells.[26] In keeping with the findings from conventional mice, mono-infection of *S. anginosus* in germ-free mice also induced the development of mucinous metaplasia, implying that *S. anginosus* itself, but not its interaction with gastric microbiome, is sufficient to drive gastric tumorigenesis. Beyond its intrinsic oncogenic effect, *S. anginosus* infection at the precancerous stage causes a rise in gastric pH and an altered gastric microbiota, with enrichment of pathogenic oral commensals (*Prevotella* and *Aggregatibacter*) and depletion of probiotic *B. pseudolongum*. Gastric dysbiosis due to *S. anginosus* infection might thus contribute to a pro-inflammatory and pro-tumorigenic microenvironment in the stomach. Corroborating our results, fecal transplantation of human GC microbiome to germ-free mice initiates a series of premalignant changes.[27] These findings highlight *S. anginosus* as a non-*H. pylori* pathogenic bacterium driving gastritis and precancerous atrophy-metaplasia-dysplasia sequence, concomitant with reprogrammed gastric microbiome in the murine stomach.

To further investigate the cancer-promoting potential of *S. anginosus*, we next evaluated its effect on YTN16 allografts and MNU-induced spontaneous gastric carcinogenesis. In both mouse experiments, *S. anginosus* significantly promoted GC development. *S. anginosus* boosted the growth rate of YTN16 allografts in both subcutaneous and orthotopic cancer models, and *S. anginosus* treatment in the MNU model aggravated dysplastic transformation with higher gastric tumor

(H and I) (H) Representative images of tumors, (I) tumor weight, and tumor/body weight ratio from BHI or *S. anginosus*-infected group.
(J) N-Methyl-N-nitrosourea (MNU)-induced gastric cancer model. C57BL/6 mice were treated with 5 cycles of MNU (240 ppm) treatment in alternate weeks, followed by gavage with *S. anginosus* (every 3 days, n = 11), *H. pylori SS1* (every 3 days, total for 5 doses within 2 weeks, n = 18), or BHI broth (every 3 days, n = 13) until week 36.
(K) Representative images of stomach from BHI and *S. anginosus*-infected mice showed adenoma in the antrum site; scale bars, 50 mm. Tumor incidence was higher in both *S. anginosus*- and *H. pylori*-infected mice.
(L) Tumor multiplicity and tumor size were higher in *S. anginosus*-infected mice compared with BHI broth group.
(M) Representative images of H&E staining of stomach from BHI and *S. anginosus*-infected MNU mice; scale bars, 100 μm. Pathological diagnosis showed a higher proportion of high-grade dysplasia in *S. anginosus*-monocolonizaed MNU mice.
(N) Ki-67 staining showed increased proliferation rates in *S. anginosus*-infected mice compared with BHI broth group; scale bars, 50 μm. Data were shown as mean ± SEM. Each spot represents one subject. Two-way ANOVA (B), chi-squared ($\chi^2$) test (K), Mann-Whitney U test (L/tumor number), and Student's t test (D–F, I, L/tumor size, and N) were used to examine the statistical significance between groups.
See also Figure S4 and Table S6.

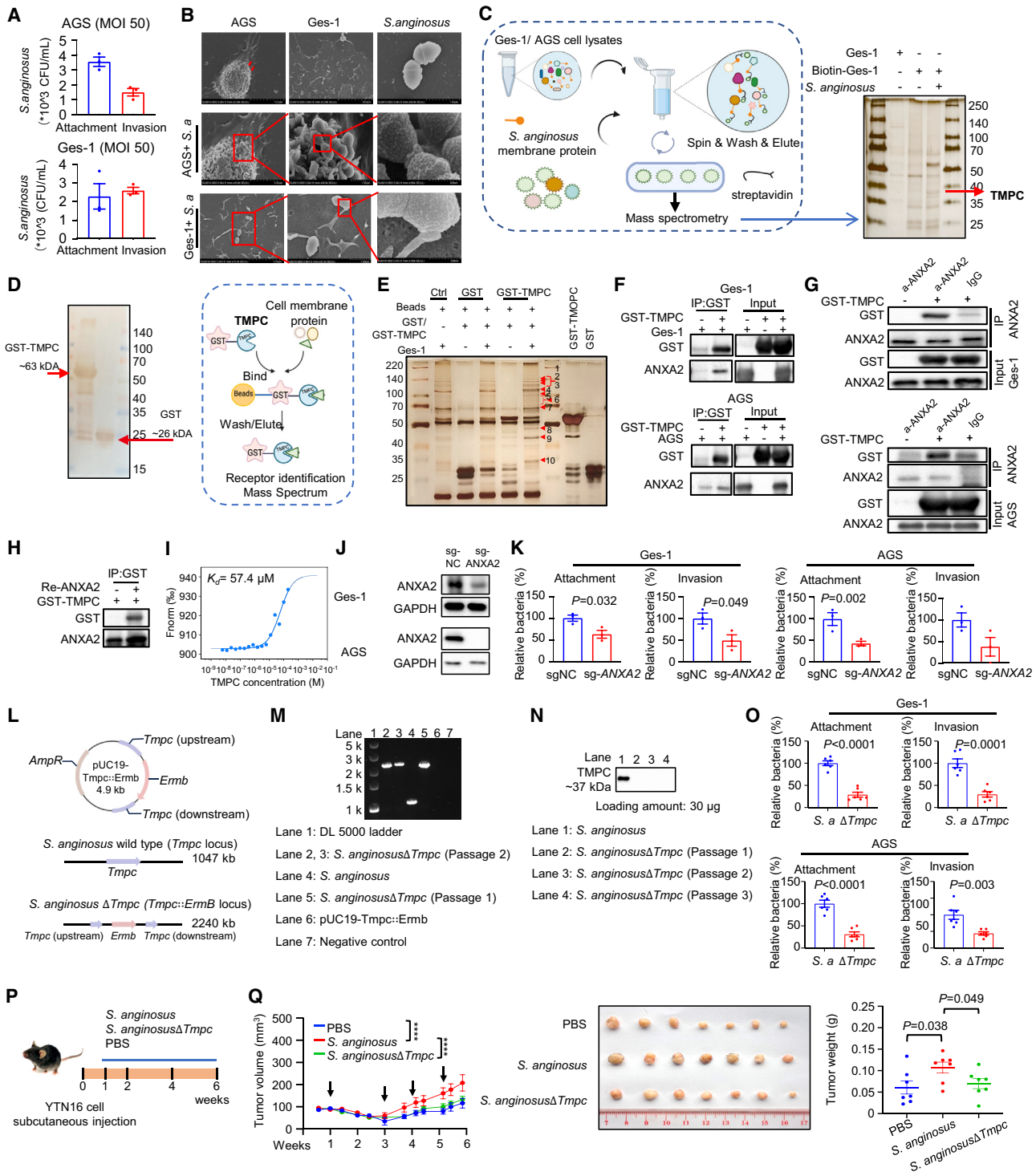


**Figure 6. *Streptococcus anginosus* interacts with gastric epithelial cells through a TMPC-Annexin A2 (ANXA2) axis**

(A) Bacteria attachment and invasion assay showed that *S. anginosus* attached onto and invaded into AGS and Ges-1 cells after co-culture (n = 3 per group).

(B) Representative scanning electron microscopy (SEM) images of AGS and Ges-1 cells after co-culture with *S. anginosus*. The higher magnification images showed attachment between bacteria and the cells.

(C) TMPC, a 37 kDa protein located on the surface of *S. anginosus*, was identified by silver staining in combination with mass spectrometry analysis after biotin pull-down assay.

*(legend continued on next page)*

incidence, especially for high-grade, locally invasive dysplasia. In line with its tumor-promoting effect, *S. anginosus* infection drives increased cell proliferation in the gastric mucosa and tumors. In addition, we showed that *S. anginosus* infection impairs gastric barrier function, as indicated by the time-dependent reductions in the expression of tight junction markers CLDN18, OCLN, and ZO-1. Tight junction is critical for maintaining cellular polarity, and its disruption is a hallmark of epithelial tumorigenesis. For instance, the loss of CLDN18, a unique tight junction protein in stomach, results in spontaneous neoplasia and tumorigenesis in mice.[28,29] Impaired cell-cell tight junctions also favor bacterial adhesion and invasion into gastric mucosal epithelial cells, allowing the establishment of persistent colonization and damage to gastric mucosa.[30] Our results collectively indicate that *S. anginosus* accelerates gastric tumorigenesis by promoting cell proliferation and disrupting gastric barrier integrity.

Bacterial adherence is frequently the prerequisite step to the initiation of tumorigenesis. In light of the oncogenic role of *S. anginosus* in the gastric epithelium, we elucidated the direct interplay between *S. anginosus* and gastric epithelium. *S. anginosus* readily attached and invaded gastric epithelial cells. We identified an *S. anginosus* surface adhesin, TMPC, which directly interacts with gastric epithelial cell receptors as observed in the pull-down assay. Reciprocal IP demonstrated that TMPC functions as a ligand for ANXA2 expressed on gastric cells. Experiments with recombinant TMPC and ANXA2 validate their direct interaction with an apparent $K_d$ of 57.4 μM. This interaction is essential for the tumorigenic function of *S. anginosus*, as the genetic ablation of TMPC abolished attachment, invasion, and tumorigenicity of *S. anginosus*. Consistent with these observations, TMPC was reported to be required for *S. pneumoniae*-associated lung infection and virulence,[31] indicating a pathogenic role of this protein in *Streptococcus* colonization in humans. On the other hand, knockout of its corresponding receptor, ANXA2, in human GC cells largely reduced *S. anginosus* attachment and invasion into gastric epithelial cells. In agreement with our results, ANXA2 has been identified as a receptor for other bacteria such as *Escherichia coli*[32] and *Pseudomonas aeruginosa*.[33] Taken together, *S. anginosus* interacts with host gastric epithelial cells primarily via a TMPC-ANXA2 protein complex.

Interaction between *S. anginosus* and gastric epithelial cells then initiates oncogenic signaling cascades. Transcriptome profiling and Kyoto Encyclopedia of Genes and Genomes (KEGG) analysis revealed significant enrichment of the MAPK signaling in *S. anginosus*-infected mice. MAPK has been implicated in GC progression via the activation of the following three subfamilies: ERK, JNK, and p-38 kinase.[34–36] ERK plays vital roles in promoting cell proliferation, while JNK and p38 are closely related to apoptosis and inflammation.[37] *S. anginosus* induced the phosphorylation of ERK and JNK in gastric cells *in vitro* and *in vivo* as shown by western blot. This in turn activated downstream targets such as p-AKT, Cyclin D1, c-Myc, and c-Jun that play important roles in the regulation of cell survival, proliferation, and apoptosis. Furthermore, the depletion of *ANXA2* abolished the *S. anginosus*-mediated p-ERK, p-AKT, and p-JNK activation in gastric epithelial cells, thereby establishing the significance of TMPC-ANXA2 interplay functioning upstream of MAPK activation and pro-tumorigenic effect of this bacterium. Supporting the role of ANXA2 as a pro-tumorigenic factor, previous studies have shown that ANXA2 promotes RalA-dependent ERK1/2 signaling[38] and activates the JNK-p53 pathway.[39]

In summary, we identified *S. anginosus* as the *non-H. pylori* bacterium promoting gastric tumorigenesis. *S. anginosus* infection spontaneously initiates gastritis and precancerous atrophy-metaplasia-dysplasia sequence and accelerates gastric tumorigenesis in mouse models. We elucidated that the virulent surface factor TMPC from *S. anginosus* binds to ANXA2 on gastric epithelial cells to elicit bacteria attachment, invasion, and the downstream activation of oncogenic MAPK signaling. Our study thus provides the evidence of *S. anginosus* as a causal pathogen in the stages of gastric carcinogenesis.

## Limitations of the study

This study has some limitations. First, while we have elucidated the interaction between *S. anginosus* and host GC, its potential interplay with other cells in the tumor microenvironment such as immune cells and fibroblasts should be considered in future studies. Second, whether *S. anginosus* can work in concert with other GC-enriched pathogens or be antagonized by

(D and E) Ges-1 membrane protein was incubated with GST or GST-TMPC together with GST magnetic beads for GST-pull-down assay. Corresponding bands in GST-TMPC and Ges-1 cell membrane proteins group were subjected to mass spectrometry analysis.
(F) ANXA2 from Ges-1 and AGS cell lysates was pulled down by GST-TMPC according to the GST pull-down assay.
(G) Immunoprecipitation of ANXA2 from Ges-1 or AGS cells lysates also showed positive binding between ANXA2 and GST-TMPC.
(H) Recombinant ANXA2 and GST-TMPC directly binds to each other, as determined by GST pull-down.
(I) Microscale thermophoresis (MST) analysis of the binding affinity of TMPC to ANXA2 with a dissociation constant ($K_d$) of 57.4 μM.
(J and K) Knockout of *ANXA2* in Ges-1 or AGS cells significantly decreased *S. anginosus* attachment and invasion to the epithelial cell (n = 3 per group).
(L) The schematic representation of the insertional inactivation of *Tmpc* in *S. anginosus*. Plasmid pUC19-Tmpc::Ermb was constructed and transformed into *S. anginosus* for homologous recombination.
(M) PCR analysis of insertion mutants of *S. anginosus*. Bacteria chromosomal DNA was used as template for the PCR. Primer *Tmpc*-F/R were used to validate *Ermb* insertion.
(N) Analysis of TMPC protein level of *S. anginosus* and *S. anginosus*Δ*Tmpc*.
(O) *S. anginosus*Δ*Tmpc* showed decreased adhesion and invasion ability compared with *S. anginosus* wild type (n = 6 per group).
(P) C57BL/6 mice were intratumorally injected with *S. anginosus* ($10^5$ CFU, n = 7), *S. anginosus*Δ*Tmpc* ($10^5$ CFU, n = 7), or PBS (n = 7, 50 μL) once a week in YTN16 allograft model of GC.
(Q) Tumor growth curve (arrows indicated *S. anginosus* injection), images of tumors, and tumor weight from *S. anginosus*-, *S. anginosus*Δ*Tmpc*-, or PBS-injected YTN16 allografts. Data were shown as mean ± SEM. Each spot represents one subject. Two-way ANOVA (Q) and Student's t test (K, O, Q) were used to examine the statistical significance between groups. ****$p < 0.0001$.
See also Figure S5 and Table S8.

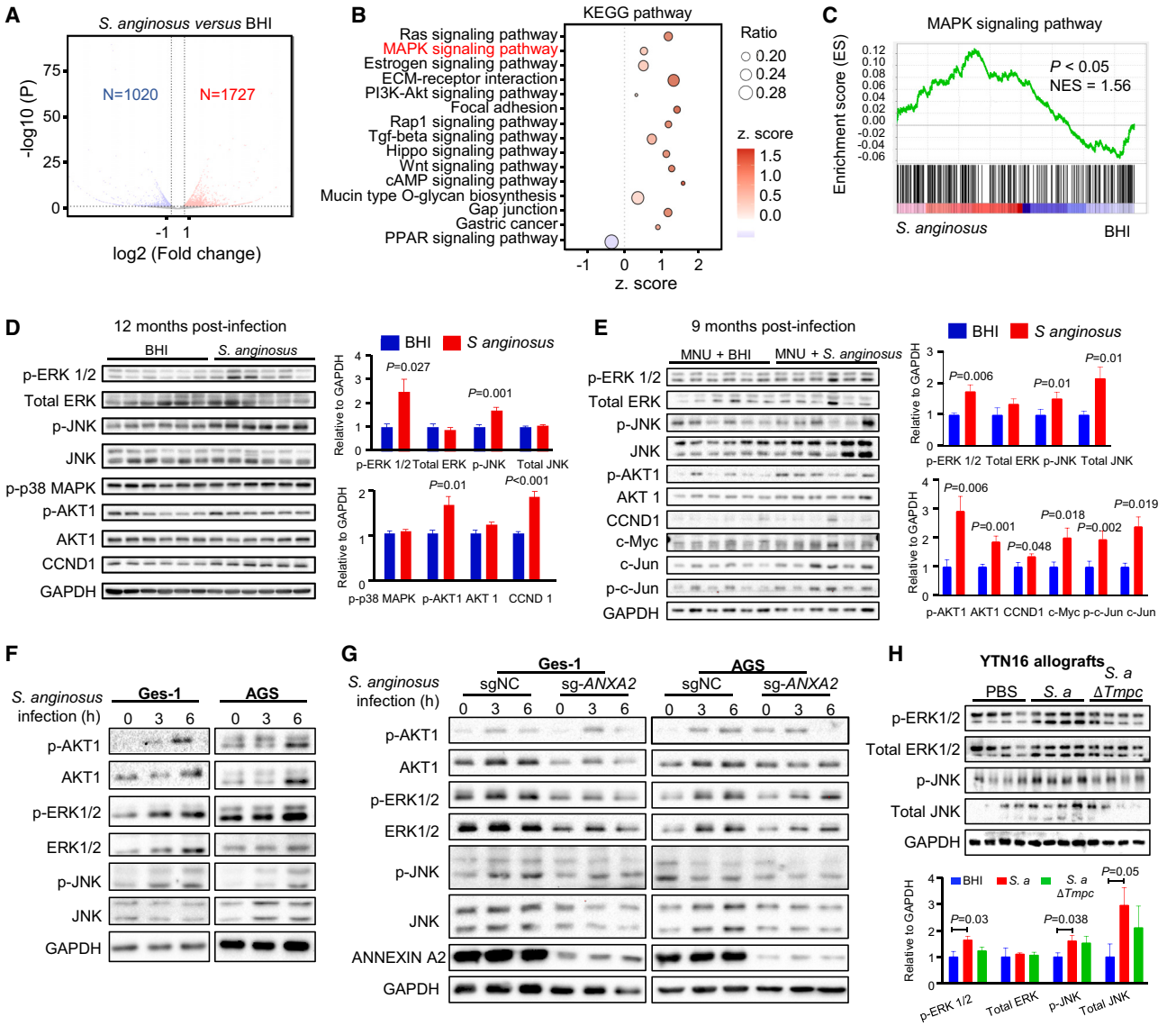


**Figure 7. *Streptococcus anginosus* activates MAPK signaling via TMPC-ANXA2 axis**

(A) Volcano plot of RNA sequencing dataset showing differential expressed genes (DEGs) in the stomach from *S. anginosus*-infected mice (n = 3) compared with BHI control mice (n = 3) at 12 months ($p < 0.05$, fold-change [FC] $\geq 1.5$). Results were derived from biological triplicates.

(B) KEGG pathway enrichment analysis of DEGs from RNA sequencing dataset. Size of circles represents the ratio of DEGs in pathways. Red: upregulated, blue: downregulated.

(C) Gene set enrichment analysis (GSEA) showing the enrichment of Ras and MAPK signaling pathways.

(D) Western blot analysis of the activation of MAPK pathway in *S. anginosus*-infected mice compared with BHI control group of conventional mice at 12 months post-infection, with increased p-ERK, p-JNK, and p-AKT, and downstream Cyclin D1 (n = 6 per group).

(E) *S. anginosus* activated MAPK signaling pathway in MNU-induced gastric tumorigenesis model at 9 months post-infection, with increased downstream c-Myc and c-Jun (n = 6 per group).

(F) *S. anginosus* activated MAPK signaling in Ges-1 and AGS cells after co-culture for 6 h (n = 3 per group).

(G) *ANXA2* knockout reversed *S. anginosus*-activated MAPK signaling pathway (n = 3 per group).

(H) TMPC protein depletion abolished *S. anginosus*-induced MAPK signaling activation in YTN16 allograft gastric cancer model (n = 4 per group). Data were shown as mean ± SEM. Each lane of western blotting picture represents one subject. The Student's t test (D, E, and H) was used to examine the statistical significance between groups.

See also Figure S6.

probiotic bacteria during GC progression also deserves further investigation. Despite these limitations, our study provided the evidence of a non-*H. pylori* microbe that could contribute to GC development.

## STAR★METHODS

Detailed methods are provided in the online version of this paper and include the following:

- KEY RESOURCES TABLE
- RESOURCE AVAILABILITY
  - Lead contact
  - Materials availability
  - Data and code availability
- EXPERIMENTAL MODEL AND STUDY PARTICIPANT DETAILS
  - Mouse models
  - Subject, bacteria, and cell line details
- METHODS DETAILS
  - Histological evaluation
  - Fluorescence in Situ Hybridization (FISH)
  - Live bacteria culture from mice stomach
  - Serum Alanine Transaminase (ALT), Aspartate aminotransferas (AST) and creatinine detection
  - Mouse gastric pH detection
  - Alcian blue staining
  - Immunohistochemistry (IHC) staining
  - Immunofluorescence (IF) staining
  - FITC-dextran permeability assay
  - 16S rRNA sequencing and data analysis
  - Single-cell RNA sequencing (scRNA-seq) and data analysis
  - Bacterial attachment and invasion assay
  - PCR array
  - Western blots
  - RNA sequencing (RNA-seq) and analysis
  - Scanning electron microscopy (SEM)
  - Quantitative PCR of *Tmpc* gene in *S. anginosus*
  - Biotin pull-down assay
  - GST pull-down assay
  - Co-immunoprecipitation (Co-IP)
  - Microscale thermophoresis (MST)
  - Knockout of *ANXA2* by CRISPR-Cas9
  - Construction of *S. anginosusΔTmpc*
- QUANTIFICATION AND STATISTICAL ANALYSIS
  - Statistical analysis

## SUPPLEMENTAL INFORMATION

Supplemental information can be found online at https://doi.org/10.1016/j.cell.2024.01.004.

## ACKNOWLEDGMENTS

This study was supported by National Key R&D Program of China (no. 2020YFA0509200/2020YFA0509203), RGC Theme-based Res Scheme Hong Kong (T21-705/20-N),RGC Collaborative Research Fund (C4039-19GF, C7065-18GF), RGC Research Impact Fund (R4032-21F), RGC-GRF Hong Kong (14163817), and Vice-Chancellor's Discretionary Fund CUHK. The authors thank Prof. Sachiyo Nomura (University of Tokyo, Japan) for the gift of YTN16 cell line, Prof. Barbara Spellerberg (Institute of Medical Microbiology and Hospital Hygiene, University of Ulm, Germany) for providing us with p919 plasmid.

## AUTHOR CONTRIBUTIONS

K.F. performed experiments and drafted the manuscript. A.H.K.C. and K.F.T. performed histological evaluation as pathologists. W.L., K.Y., and O.O.C. performed bioinformatic analyses. Y.Z., F.W., P.H., Y.P., and D.C. assisted on mouse experiments. N.M.L. assisted on microscale thermophoresis assay. M.G. and H.H. assisted on plasmid construction. C.C.W. and X.Z. commented on the study and revised the paper. J.J.Y.S. co-supervised the study. J.Y. designed and supervised the study and revised the manuscript.

## DECLARATION OF INTERESTS

The authors declare no competing interests.

Received: August 8, 2022
Revised: October 13, 2023
Accepted: January 2, 2024
Published: January 30, 2024

## REFERENCES

1. Sung, H., Ferlay, J., Siegel, R.L., Laversanne, M., Soerjomataram, I., Jemal, A., and Bray, F. (2021). Global Cancer Statistics 2020: GLOBOCAN Estimates of Incidence and Mortality Worldwide for 36 Cancers in 185 Countries. CA Cancer J. Clin. *71*, 209–249.
2. Uemura, N., Okamoto, S., Yamamoto, S., Matsumura, N., Yamaguchi, S., Yamakido, M., Taniyama, K., Sasaki, N., and Schlemper, R.J. (2001). Helicobacter pylori infection and the development of gastric cancer. N. Engl. J. Med. *345*, 784–789.
3. Marshall, B.J., and Warren, J.R. (1984). Unidentified curved bacilli in the stomach of patients with gastritis and peptic ulceration. Lancet *1*, 1311–1315.
4. Lofgren, J.L., Whary, M.T., Ge, Z., Muthupalani, S., Taylor, N.S., Mobley, M., Potter, A., Varro, A., Eibach, D., Suerbaum, S., et al. (2011). Lack of commensal flora in Helicobacter pylori-infected INS-GAS mice reduces gastritis and delays intraepithelial neoplasia. Gastroenterology *140*, 210–220.
5. Coker, O.O., Dai, Z., Nie, Y., Zhao, G., Cao, L., Nakatsu, G., Wu, W.K., Wong, S.H., Chen, Z., Sung, J.J.Y., et al. (2018). Mucosal microbiome dysbiosis in gastric carcinogenesis. Gut *67*, 1024–1032.
6. Whiley, R.A., and Beighton, D. (1991). Emended Descriptions and Recognition of Streptococcus Constellatus, Streptococcus Intermedius, and Streptococcus Anginosus as Distinct Species. Int. J. Syst. Bacteriol. *41*, 1–5.
7. Hamada, S., and Slade, H.D. (1980). Biology, immunology, and cariogenicity of Streptococcus mutans. Microbiol. Rev. *44*, 331–384.
8. Sasaki, M., Kodama, Y., Shimoyama, Y., Ishikawa, T., and Kimura, S. (2018). Aciduricity and acid tolerance mechanisms of Streptococcus anginosus. J. Gen. Appl. Microbiol. *64*, 174–179.
9. Sung, J.J.Y., Coker, O.O., Chu, E., Szeto, C.H., Luk, S.T.Y., Lau, H.C.H., and Yu, J. (2020). Gastric microbes associated with gastric inflammation, atrophy and intestinal metaplasia 1 year after Helicobacter pylori eradication. Gut *69*, 1572–1580.
10. Ferreira, R.M., Pereira-Marques, J., Pinto-Ribeiro, I., Costa, J.L., Carneiro, F., Machado, J.C., and Figueiredo, C. (2018). Gastric microbial community profiling reveals a dysbiotic cancer-associated microbiota. Gut *67*, 226–236.
11. Yu, G., Torres, J., Hu, N., Medrano-Guzman, R., Herrera-Goepfert, R., Humphrys, M.S., Wang, L., Wang, C., Ding, T., Ravel, J., et al. (2017).

Molecular Characterization of the Human Stomach Microbiota in Gastric Cancer Patients. Front. Cell. Infect. Microbiol. *7*, 302.

12. Houghton, J.M. (2012). Introduction. In Helicobacter Species Methods and Protocols, *921* (Springer), pp. 1–5.
13. Banks, M., Graham, D., Jansen, M., Gotoda, T., Coda, S., di Pietro, M., Uedo, N., Bhandari, P., Pritchard, D.M., Kuipers, E.J., et al. (2019). British Society of Gastroenterology guidelines on the diagnosis and management of patients at risk of gastric adenocarcinoma. Gut *68*, 1545–1575.
14. Petersen, C.P., Mills, J.C., and Goldenring, J.R. (2017). Murine Models of Gastric Corpus Preneoplasia. Cell. Mol. Gastroenterol. Hepatol. *3*, 11–26.
15. Wessler, S., and Backert, S. (2008). Molecular mechanisms of epithelial-barrier disruption by Helicobacter pylori. Trends Microbiol. *16*, 397–405.
16. Frank, J.A. (2012). Claudins and alveolar epithelial barrier function in the lung. Ann. N. Y. Acad. Sci. *1257*, 175–183.
17. Niimi, T., Nagashima, K., Ward, J.M., Minoo, P., Zimonjic, D.B., Popescu, N.C., and Kimura, S. (2001). claudin-18, a novel downstream target gene for the T/EBP/NKX2.1 homeodomain transcription factor, encodes lung- and stomach-specific isoforms through alternative splicing. Mol. Cell. Biol. *21*, 7380–7390.
18. Sun, J.H., Li, X.L., Yin, J., Li, Y.H., Hou, B.X., and Zhang, Z. (2018). A screening method for gastric cancer by oral microbiome detection. Oncol. Rep. *39*, 2217–2224.
19. Hu, Y.L., Pang, W., Huang, Y., Zhang, Y., and Zhang, C.J. (2018). The Gastric Microbiome Is Perturbed in Advanced Gastric Adenocarcinoma Identified Through Shotgun Metagenomics. Front. Cell. Infect. Microbiol. *8*, 433.
20. Huang, K.K., Ma, H., Chong, R.H.H., Uchihara, T., Lian, B.S.X., Zhu, F., Sheng, T., Srivastava, S., Tay, S.T., Sundar, R., et al. (2023). Spatiotemporal genomic profiling of intestinal metaplasia reveals clonal dynamics of gastric cancer progression. Cancer Cell *41*, 2019–2037.e8.
21. Yamamoto, M., Nomura, S., Hosoi, A., Nagaoka, K., Iino, T., Yasuda, T., Saito, T., Matsushita, H., Uchida, E., Seto, Y., et al. (2018). Established gastric cancer cell lines transplantable into C57BL/6 mice show fibroblast growth factor receptor 4 promotion of tumor growth. Cancer Sci. *109*, 1480–1492.
22. Busuttil, R.A., Liu, D.S., Di Costanzo, N., Schröder, J., Mitchell, C., and Boussioutas, A. (2018). An orthotopic mouse model of gastric cancer invasion and metastasis. Sci. Rep. *8*, 825.
23. Deka, R.K., Brautigam, C.A., Yang, X.F., Blevins, J.S., Machius, M., Tomchick, D.R., and Norgard, M.V. (2006). The PnrA (Tp0319; TmpC) lipoprotein represents a new family of bacterial purine nucleoside receptor encoded within an ATP-binding cassette (ABC)-like operon in Treponema pallidum. J. Biol. Chem. *281*, 8072–8081.
24. Jerabek-Willemsen, M., André, T., Wanner, R., Roth, H.M., Duhr, S., Baaske, P., and Breitsprecher, D. (2014). MicroScale Thermophoresis: Interaction analysis and beyond. J. Mol. Struct. *1077*, 101–113.
25. Correa, P. (1992). Human gastric carcinogenesis: a multistep and multifactorial process–First American Cancer Society Award Lecture on Cancer Epidemiology and Prevention. Cancer Res. *52*, 6735–6740.
26. Bockerstett, K.A., Lewis, S.A., Wolf, K.J., Noto, C.N., Jackson, N.M., Ford, E.L., Ahn, T.H., and DiPaolo, R.J. (2020). Single-cell transcriptional analyses of spasmolytic polypeptide-expressing metaplasia arising from acute drug injury and chronic inflammation in the stomach. Gut *69*, 1027–1038.
27. Kwon, S.K., Park, J.C., Kim, K.H., Yoon, J., Cho, Y., Lee, B., Lee, J.J., Jeong, H., Oh, Y., Kim, S.H., et al. (2022). Human gastric microbiota transplantation recapitulates premalignant lesions in germ-free mice. Gut *71*, 1266–1276.
28. Suzuki, K., Sentani, K., Tanaka, H., Yano, T., Suzuki, K., Oshima, M., Yasui, W., Tamura, A., and Tsukita, S. (2019). Deficiency of Stomach-Type Claudin-18 in Mice Induces Gastric Tumor Formation Independent of H pylori Infection. Cell. Mol. Gastroenterol. Hepatol. *8*, 119–142.
29. Caron, T.J., Scott, K.E., Sinha, N., Muthupalani, S., Baqai, M., Ang, L.H., Li, Y., Turner, J.R., Fox, J.G., and Hagen, S.J. (2021). Claudin-18 Loss Alters Transcellular Chloride Flux but not Tight Junction Ion Selectivity in Gastric Epithelial Cells. Cell. Mol. Gastroenterol. Hepatol. *11*, 783–801.
30. Wroblewski, L.E., and Peek, R.M. (2011). "Targeted disruption of the epithelial-barrier by Helicobacter pylori". Cell Commun. Signal. *9*, 29.
31. Abdullah, M.R., Batuecas, M.T., Jennert, F., Voß, F., Westhoff, P., Kohler, T.P., Molina, R., Hirschmann, S., Lalk, M., Hermoso, J.A., et al. (2021). Crystal Structure and Pathophysiological Role of the Pneumococcal Nucleoside-binding Protein PnrA. J. Mol. Biol. *433*, 166723.
32. Li, X., Pei, G., Zhang, L., Cao, Y., Wang, J., Yu, L., Dianjun, W., Gao, S., Zhang, Z.S., Yao, Z., et al. (2019). Compounds targeting YadC of uropathogenic Escherichia coli and its host receptor annexin A2 decrease bacterial colonization in bladder. EBioMedicine *50*, 23–33.
33. Kirschnek, S., Adams, C., and Gulbins, E. (2005). Annexin II is a novel receptor for Pseudomonas aeruginosa. Biochem. Biophys. Res. Commun. *327*, 900–906.
34. Akter, H., Park, M., Kwon, O.S., Song, E.J., Park, W.S., and Kang, M.J. (2015). Activation of matrix metalloproteinase-9 (MMP-9) by neurotensin promotes cell invasion and migration through ERK pathway in gastric cancer. Tumour Biol. *36*, 6053–6062.
35. Han, H., Lim, J.W., and Kim, H. (2019). Lycopene Inhibits Activation of Epidermal Growth Factor Receptor and Expression of Cyclooxygenase-2 in Gastric Cancer Cells. Nutrients *11*, 2213.
36. Li, W., Fan, M., Chen, Y., Zhao, Q., Song, C., Yan, Y., Jin, Y., Huang, Z., Lin, C., and Wu, J. (2015). Melatonin Induces Cell Apoptosis in AGS Cells Through the Activation of JNK and P38 MAPK and the Suppression of Nuclear Factor-Kappa B: a Novel Therapeutic Implication for Gastric Cancer. Cell. Physiol. Biochem. *37*, 2323–2338.
37. Keshet, Y., and Seger, R. (2010). The MAP kinase signaling cascades: a system of hundreds of components regulates a diverse array of physiological functions. Methods Mol. Biol. *661*, 3–38.
38. Long, Y., Chong, T., Lyu, X., Chen, L., Luo, X., Faleti, O.D., Deng, S., Wang, F., He, M., Qian, Z., et al. (2022). FOXD1-dependent RalA-ANXA2-Src complex promotes CTC formation in breast cancer. J. Exp. Clin. Cancer Res. *41*, 301.
39. Feng, X., Liu, H., Zhang, Z., Gu, Y., Qiu, H., and He, Z. (2017). Annexin A2 contributes to cisplatin resistance by activation of JNK-p53 pathway in non-small cell lung cancer cells. J. Exp. Clin. Cancer Res. *36*, 123.

## STAR★METHODS

### KEY RESOURCES TABLE

| REAGENT or RESOURCE | SOURCE | IDENTIFIER |
|---|---|---|
| **Antibodies** | | |
| Donkey anti-Rabbit IgG (H+L) Highly Cross-Adsorbed Secondary Antibody, Alexa Fluor 594 | Invitrogen | Cat#A-21207; RRID: AB_141637 |
| Goat anti-Mouse IgG (H+L) Cross-Adsorbed Secondary Antibody, Alexa Fluor 488 | Invitrogen | Cat#A-11001; RRID: AB_2534069 |
| Rabbit monoclonal anti-Akt1 (clone C73H10) | Cell Signaling Technology | Cat#2938s; RRID: AB_915788 |
| Mouse monoclonal anti-Annexin A2 (clone 3H1B11) | ProteinTech | Cat#60051-1-Ig; RRID: AB_2057309 |
| Rabbit polyclonal anti-GIF | Sigma-Aldrich | Cat#HPA040774; RRID: AB_10795626 |
| Rabbit monoclonal anti-c-Jun (clone 60A8) | Cell Signaling Technology | Cat#9165; RRID: AB_2130165 |
| Rabbit polyclonal anti-Claudin 18 | Thermo Fisher Scientific | Cat#38-8100; RRID: AB_2533383 |
| Rabbit polyclonal anti-c-Myc | Cell signaling | Cat#9402; RRID: AB_2151827 |
| Rabbit polyclonal anti-Cyclin D1 | Cell signaling | Cat#2922s; RRID: AB_2228523 |
| Rabbit polyclonal anti-ERK1/2 | Santa Cruz Biotechnology | Cat#sc-292838; RRID: AB_2650548 |
| Rabbit monoclonal anti-GAPDH (clone D16H11) | Cell Signaling Technology | Cat#5174s; RRID: AB_10622025 |
| Mouse monoclonal anti-GST-Tag (clone 26H1) | Cell Signaling Technology | Cat#2624; RRID: AB_2189875 |
| Rabbit monoclonal anti-Ki-67 (clone D3B5) | Cell Signaling Technology | Cat#12202; RRID: AB_2620142 |
| Mouse monoclonal anti-Occludin (clone E-5) | Santa Cruz Biotechnology | Cat#sc-133256; RRID: AB_2156317 |
| Rabbit monoclonal anti-PCNA (clone D3H8P) | Cell Signaling Technology | Cat#13110; RRID: AB_2636979 |
| Rabbit polyclonal anti-Phospho-Akt (Ser473) | Cell Signaling Technology | Cat#9271s; RRID: AB_329825) |
| Rabbit monoclonal anti-Phospho-c-Jun (Ser73) (clone D47G9) | Cell Signaling Technology | Cat#3270; RRID: AB_2129575 |
| Rabbit monoclonal anti-Phospho-p38 MAPK (Thr180/Tyr182) (clone D3F9) | Cell Signaling Technology | Cat#4511s; RRID: AB_2139682 |
| Rabbit monoclonal anti-Phospho-p44/42 MAPK (Erk1/2) (Thr202/Tyr204) (clone 197G2) | Cell Signaling Technology | Cat#4377; RRID: AB_331775 |
| Mouse monoclonal anti- Phospho-SAPK/JNK (Thr183/Tyr185) (clone G9) | Cell Signaling Technology | Cat#9255s; RRID: AB_2307321 |
| Rabbit polyclonal anti-SAPK/JNK | Cell Signaling Technology | Cat#9252; RRID: AB_2250373 |
| Rabbit polyclonal anti-ZO-1 | Abcam | Cat#ab96587; RRID: AB_10680012 |
| Rabbit monoclonal anti-β-Actin (clone 13E5) | Cell Signaling Technology | Cat#4970; RRID: AB_2223172 |
| Rabbit polyclonal anti-TMPC | This study | N/A |
| **Bacterial and virus strains** | | |
| *Streptococcus anginosus* | ATCC | Cat#ATCC 33397 |
| *Helicobacter pylori SS1* | The Chinese University of Hong Kong | N/A |
| *Escherichia coli* | Sangon Biotech | N/A |
| *S. anginosusΔTmpc* | This study | N/A |
| **Chemicals, peptides, and recombinant proteins** | | |
| Lectin GS-II from Griffonia simplicifolia, Alexa Fluor 488 Conjugate | Invitrogen | Cat#L21415 |
| N-Methyl-N-nitrosourea | Aladdin | N136701 |
| FITC-dextran (4kDa) | Sigma-Aldrich | 46944 |
| EZ-Link™ Sulfo-NHS-LC-Biotin | Thermo Fisher Scientific | 21335B |

(*Continued on next page*)

*Continued*

| REAGENT or RESOURCE | SOURCE | IDENTIFIER |
|---|---|---|
| Recombinant GST-TMPC protein | This study | NA |
| Recombinant Annexin A2 protein | Origene | AR09353PU-N |
| Competence-stimulated peptide 1 | ChinaPeptides | EMRLSKFFRDFILQRKK |
| Erythromycin | Aladdin | E105345 |
| Sulfadiazine | MedChemExpress | Cat#HY-B0273 |
| Aztreonam | MedChemExpress | Cat#HY-B0129 |
| Gentamicin | MedChemExpress | Cat#HY-A0276A |
| **Critical commercial assays** | | |
| PrimeScript RT reagent Kit | Takara | RR037A |
| Mouse inflammatory response and autoimmunity PCR array | QIAGEN | PAMM-077Z |
| Pierce™ Silver Stain for Mass Spectrometry | Thermo Fisher Scientific | 24600 |
| His-Tag Labeling Kit Red-tris-NTA | NanoTemper Technologies | MO-L018 |
| QIAamp DNA mini kit | QIAGEN | Cat#51306 |
| **Deposited data** | | |
| RNA sequence data of mouse gastric tissues | This study | GSA: CRA014025 |
| 16S rRNA gene sequence data of gastric biopsy samples | Coker et al.[5] | N/A |
| 16S rRNA gene sequence data of gastric biopsy samples | Sung et al.[9] | N/A |
| 16S rRNA gene sequence data of gastric biopsy samples | Ferreira et al.[10] | RJNA413125 |
| 16S rRNA gene sequence data of gastric tumor samples | Yu et al.[11] | PRJNA310127 |
| **Experimental models: Cell lines** | | |
| Human: Ges-1 cells | Cell Research Institute, Shanghai | N/A |
| Human: AGS cells | ATCC | CRL-1739 |
| Human 293T cells | ATCC | CRL-3216; RRID: CVCL_0063 |
| Mouse: YTN16 cells | Gift from Prof. Sachiyo Nomura | N/A |
| Human: MKN28 cells | JCRB | JCRB0253 |
| Human: NCI-N87 cells | ATCC | CRL-5822; RRID: CVCL_1603 |
| **Experimental models: Organisms/strains** | | |
| Mouse: C57/BL6 | The Chinese University of Hong Kong | N/A |
| Mouse: Germ-free BALB/c | The Third Military Medical University | N/A |
| **Oligonucleotides** | | |
| Guide RNA targeting sequence: human ANXA2: TCACCTACCTTTGGTCTTGA | GenScript | N/A |
| Primers for PCR, see Table S1 | BGI Genomics | N/A |
| FITC-labeled *S. anginosus* probe (sequence: 5'-AGT TAA ACA GTT TCC AAA GCC TAC-3') | FOCOFISH, Guangzhou | N/A |
| **Recombinant DNA** | | |
| Plasmid pGEX-4T-1 vector | Sangon Biotech | N/A |
| Plasmid lentiCRISPRv2 vector | Addgene | Cat#108100; RRID: Addgene_108100 |
| Plasmid pUC19-Tmpc::Ermb | This study | N/A |
| Plasmid p919 vector | Gift from Prof. Barbara Spellerberg | N/A |
| **Software and algorithms** | | |
| GraphPad Prism 8.2 | GraphPad Software | www.graphpad.com |
| Image Lab version 5.2.1 | Bio-Rad | N/A |

(*Continued on next page*)

*Continued*

| REAGENT or RESOURCE | SOURCE | IDENTIFIER |
|---|---|---|
| MO Affinity Analysis v.3.0.5 | NanoTemper Technologies | N/A |
| Cell Ranger v7.2.0 | 10xgenomics | www.10xgenomics.com |
| R project | R Core Team | www.r-project.org |
| Other | | |
| *Tmpc* gene, ATCC 33397 strain | ATCC | Locus Tag EODJBPNH_00792 |

## RESOURCE AVAILABILITY

### Lead contact

Further information and requests for resources and reagents should be directed to and will be fulfilled by the lead contacts, Dr. Jun Yu (junyu@cuhk.edu.hk).

### Materials availability

Plasmids, recombinant TMPC protein, and anti-TMPC antibody generated in this study will be shared by the lead contact upon request.

### Data and code availability

- Raw data for Ferreira et al.[10] and Yu et al.[11] were retrieved form Sequence Read Archive under accession PRJNA413125 and PRJNA310127, respectively. RNA sequencing data of mosue gastric tissues has been deposited in the Genome Sequence Archive (Genomics, Proteomics & Bioinformatics 2021) in National Genomics Data Center (Nucleic Acids Res 2022), China National Center for Bioinformation / Beijing Institute of Genomics, Chinese Academy of Sciences (GSA: CRA014025). Datasets of Coker et al.[5] and Sung et al.[9] will be shared by the lead contact upon request.
- This paper does not report original code.
- Any additional information required to reanalyze the data reported in this paper is available from the lead contact upon request.

## EXPERIMENTAL MODEL AND STUDY PARTICIPANT DETAILS

### Mouse models

#### S. anginosus *infection in conventional mice*

Male C57BL/6 conventional mice (6-8 weeks old) were randomly assigned into three groups: BHI (negative control), *H. pylori SS1* (positive control), and *S. anginosus*. Mice in BHI or *S. anginosus* groups were orally given broth medium (200 μL) or bacteria ($2\times10^9$ Colony-forming units (CFU) in 200 μL BHI broth) once every three days. *H. pylori SS1*-infected mice were dosed with bacteria ($2\times10^9$ CFU in 200 μL BHI broth) for 5 times in 2 weeks to achieve successful colonization in the stomach. Mice in each group were sacrificed at 2 weeks, 3-, 6-, 9- and 12-months post-infection. For the *H. pylori SS1* and *S. anginosus* co-infection mouse model, mice were orally given both bacteria together from the first dose. All the animal experiments were approved by the Animal Experimentation Ethics Committee of The Chinese University of Hong Kong.

#### S. anginosus *infection in Germ-free mice*

For *S. anginosus* mono-colonized germ-free mice model, germ-free BALB/C male (8 weeks-old) mice were randomly divided into BHI broth control and *S. anginosus*-infected groups. Mice were orally administrated with BHI (200 μL) or *S. anginosus* ($2\times10^9$ CFU in 200 μL BHI broth) once per week and sacrificed at 9 months post-infection. All the animal experiments were approved by the Animal Experimentation Ethics Committee of The Third Military Medical University.

#### *Tumor allograft mice*

YTN16 cells were suspended in 50% Matrigel and subcutaneously implanted ($8x10^6$ cells per tumor) into male C57BL/6 mice (8 weeks-old), and randomly divided PBS and *S. anginosus* groups (n = 10 per group). PBS or *S. anginosus* ($10^5$ CFU in 50 μL PBS) were intratumorally injected every 5 days. For *S. anginosusΔTmpc*-related allograft mouse model, PBS or bacteria (*S. anginosus or S. anginosusΔTmpc*, $10^5$ CFU in 50 μL PBS, n = 7 per group) were intratumorally injected once per week. The tumor volume was measured and calculated as Length*(1/2Width).[2] To establish orthotopic tumor model, mice were anaesthetized with isoflurane and shaved around the abdomen.[22] An incision was made to expose the stomach. YTN16 cells ($5x10^6$) in 30 μL Matrigel (25% in PBS) were injected into the serosa of the stomach, followed by suturing of the incision. Mice were gavaged with *S. anginosus* ($2\times10^9$ CFU, n = 21) or BHI broth (n = 19) starting from the 2nd week after surgery and sacrificed on the 8th week. All the animal experiments were approved by the Animal Experimentation Ethics Committee of The Chinese University of Hong Kong.

### *MNU-induced gastric carcinogenesis in mice*

Male C57/BL6 mice (5-week-old) were given MNU (240 ppm, N136701, Aladdin) in drinking water for 5 alternative weeks. After the last cycle of MNU treatment, mice were gavaged with BHI broth (n =13) or *S. anginosus* (n =11) once every three days. Mice in *H. pylori* SS1 (n =18) group were orally gavaged 5 times with *H. pylori SS1* for once every three days to establish infection. Mice were sacrificed on the 36th week. All the animal experiments were approved by the Animal Experimentation Ethics Committee of The Chinese University of Hong Kong.

## Subject, bacteria, and cell line details

### *Human subjects*

The abundance of *S. anginosus* in gastric mucosa was quantified by 16s rRNA gene sequence from 311 human gastric biopsy tissues of 110 superficial gastritis (SG), 117 atrophy gastritis (AG), 45 intestinal metaplasia (IM) and 39 GC subjects.[5]

### *Bacteria*

*S. anginosus* (ATCC 33397) was obtained from the American Type Culture Collection. *S. anginosus* was cultured on BHI agar (CM1136B; Thermo Fisher Scientific) plate and grown in BHI broth (CM1135B; Thermo Fisher Scientific) medium at 37°C under aerobic condition overnight. *H. pylori SS1* was grown at Columbia blood agar (PP2001, Thermo Fisher Scientific) in an anaerobic jar with a microaerophilic environment for 3 days at 37 °C. Bacterial colonies were picked from agar plates and inoculated in BBL Brucella broth medium (PP2001, BD Biosciences) supplemented with 10% fetal bovine serum (FBS) (26140079, Thermo Fisher Scientific) and incubated at microaerophilic conditions at 37 °C for 24 h. *Escherichia coli* (*E. coli*) DH5a served as a host for pUC19-Tmpc::Ermb plasmid. The *E. coli* strain was incubated in Luria broth Miller (LB) broth supplemented with 400 ug/mL erythromycin. *S. anginosusΔTmpc* were incubated in the presence of 5 ug/mL erythromycin.

### *Cell lines*

Human gastric cell lines AGS and NCI-N87 were obtained from American Type Culture Collection (ATCC). Human gastric cell line MKN28 was obtained from Japanese Collection of Research Bioresources (JCRB). Human gastric cell lines Ges-1 were obtained from Cell Research Institute, Shanghai. AGS and Ges-1 cell lines were cultured in Dulbecco's Modified Eagle's Medium (DMEM) medium (11965092, Thermo Fisher Scientific). MKN28 and NCI-N87 were cultured in Rosewell Park Memorial Institute (RPMI) 1640 Medium (61870036, Thermo Fisher Scientific). All cells cultured medium were supplemented with 10% FBS, 1% Penicillin-Streptomycin solution (15070063, Thermo Fisher Scientific). Mouse YTN16 gastric cancer cell line was a gift from Prof. Sachiyo Nomura of the University of Tokyo. YTN16 was cultured as described.[21] All these cell lines were cultured in a humidified atmosphere containing 5% $CO_2$.

## METHODS DETAILS

### Histological evaluation

Mice stomach was cut along the greater curvature and washed with cold PBS (pH 7.4). Non-glandular regions were removed and the stomach was cut into fragments, each comprising the body and antrum region. Two non-adjacent fragments of the stomach (2-3 mm thick) were fixed in fresh prepared 10% formalin solution. Paraffin-embedded gastric sections (4 μm) were stained for H&E and reviewed by an experienced pathologist.

### Fluorescence in Situ Hybridization (FISH)

FITC-labeled *S. anginosus* probe (sequence: 5'-AGT TAA ACA GTT TCC AAA GCC TAC-3') was used to detect *S. anginosus* colonization in paraffin-embedded gastric sections. After deparaffinization and rehydration, specimens were treated with 0.2 N HCl and Proteinase K for 10 min for each step. Following incubation with blocking buffer on 55 °C for 2 h, FITC-labeled *S. anginosus* probe (1:50 in 35% hybridization buffer, pre-heated at 88 °C for 3 min before use) was added and hybridized in a dark, humid chamber at 42 °C overnight. Specimens were washed in wash solution (20 mM Tris-HCl, pH=7.2; 40 mM NaCl) and mounted with DAPI-antifade solution (P36931, Thermo Fisher Scientific). Images were acquired with a fluorescent microscope (Leica).

### Live bacteria culture from mice stomach

Fresh mouse gastric tissue was homogenized with 50% BHI-glycerol medium (300 μL) and series dilution (5 and 25 fold dilution) were made for bacteria culture with blank BHI agar or antibiotics-supplemented (Sulfadiazine 1mg/mL, Aztreonam 0.2 mg/mL in Tryptic Soy Broth (257371, BD Biosciences) TSA agar. Bacteria colony were picked for MALDI-TOF mass spectrum (MS) analysis to validate live *S. anginosus* (Table S3). Colony PCR and Sanger sequencing were conducted to verify the MS results.

### Serum Alanine Transaminase (ALT), Aspartate aminotransferas (AST) and creatinine detection

Serum ALT, AST and creatinine were assessed by Catalyst One Chemistry Analyzer (IDEXX Laboratories) following the manufacture's instruction. Fifty microlitres of serum was diluted to 200 μL with PBS. Diluted serum and slides for ALT, AST and creatinine were loaded together for automatic analysis.

### Mouse gastric pH detection

Prior to sacrifice, mice were deprived of food for 6 hours. Stomach was removed immediately and cut from the greater curvature. Stomach was rinsed in 2 mL saline, and the collected contents were centrifuged (4000 rpm, 10 mins, 4 °C). Thereafter, the obtained supernatant was used for gastric pH measurement with pH meter (8302BNUMD, Thermo Fisher Scientific).

### Alcian blue staining

Paraffin-embedded gastric sections were deparaffinized in xylene and rehydrated on gradient alcohol solution. Gastric sectional slides were firstly incubated with 3% acetic acid for 10 min and then stained in Alcian-blue solution (1% Alcian blue in 3% acetic acid) for 30 min. After counterstain in nuclear fast red for 10 min, slides were washed in running tap water, dehydrated in gradient ethanol, and mounted with DPX Mountant (06522, Sigma).

### Immunohistochemistry (IHC) staining

Ki-67 (12202, Cell Signaling Technology) and proliferating cell nuclear antigen (PCNA)(2586, Cell Signaling Technology) IHC was performed on paraffin-embedded sections (4 μm). The proliferation index was calculated by percentage positive cells. At least 5 random fields from corpus to antrum sites were counted for each mouse under 100X magnification.

### Immunofluorescence (IF) staining

Claudin18 (38-8100, Invitrogen), GIF (HPA040774, Sigma) and GSII (L21415, Thermo Fisher Scientific) IF staining were performed on paraffin-embedded gastric tissue sections (4 μm). Images were acquired with a fluorescent microscope (Leica).

### FITC-dextran permeability assay

MKN28 and NCI-N87 cells were seeded on 12-well transwell inserts; 0.4 μm pore size tissue culture inserted (CLS3460, Corning Costar). Cell was cultured for another 7 days after reaching confluence and medium was changed every day. MKN28 or NCI-N87 monolayer cells were infected with *S. anginosus* for 30 mins and washed by PBS for 3 times. FITC-dextran (4kDa, 1 mg/mL in Hanks' Balanced Salt Solution (HBSS) buffer, 46944, Sigma) was added into the insert. The transepithelial flux FITC-dextran were measured with excitation λ 485 nm and emission λ 535 nm.

### 16S rRNA sequencing and data analysis

Mice gastric tissues were disrupted by beads-beating after digestion with mutanolysin and lysozyme. DNA extraction was performed with QIAamp DNA mini kit. DNA library preparation and 16S ribosomal RNA gene sequencing were performed by NovoGene, Tianjin, China. The V3-V4 regions of 16S rRNA genes were amplified using specific primer (341F [CCTAYGGGRBGCASCAG] and 806R [GGACTACNNGGGTATCTAAT]) together with the barcode. The 16S rRNA gene sequence data were quality-filtered and analyzed using QIIME2 (version 2019.4.0; default parameters) software. Briefly, the sequencing errors and replicated sequences were detected by Deblur algorithm with default parameters. Before dereplicating sequences that encoded the amplicon sequence variants (ASV), paired reads were joined and trimmed to 450 base pairs. After filtering chimera sequences, the dereplicated sequences were classified taxonomically using Greengenes 16S rRNA gene reference database at a 99% identity cut-off by VSEARCH software. Differentially enriched microbes were analyzed using ALDEx2 (default parameters), a compositional-oriented method that infers technical and statistical errors by integrating the Bayesian methods. Microbial interplays were inferred by SparCC method. Correlation coefficients between taxon were estimated by setting an average of inference iterations to 100, which generated 10,000 simulated datasets to calculate the corresponding empirical *P* values (Table S5).

### Single-cell RNA sequencing (scRNA-seq) and data analysis

Tumor tissues from stomach of YTN16-induced orthotropic gastric cancer mouse model. Briefly, tumor tissues were cut into 1-3 $mm^3$ and digested with Enzyme cocktail with Tumor dissociation kit (130-090-730, Mitenyi Biotec). Dissociated single cells were sorted by FITC anti-mouse CD45 (103108, Biolegend) and dead cell marker PI with Nanocellect WOLF Cell Sorter. CD45 negative cells and CD45 positive cells were subjected to following single-cell transcriptome sequencing analysis.

ScRNA-seq data was analyzed using the 10× Genomics software package Cell Ranger version 7.1.0. The data were mapped to the mm10 reference genome supplied by 10× Genomics. A gene count matrix was generated from unique molecular identifiers (UMIs) by Cell Ranger. The data matrix was normalized for sequencing depth by dividing by the total number of UMIs for each cell and then transformed to a log scale using the R package Seurat. After normalization, the cells were split into immune and non-immune cells based on the gene *Ptprc* (Cd45) and further screened epithelial cell by gene *Epcam*. The tumor cell was identified marker gene expression: *Chga*, *Chgb*, *Pgc*, *Muc5ac*, *Col3a1*, *Cdh17*, *Pdgfrb*, *Cldn4*, *Tff3*, *Cldn7*. Differentially expressed genes (DEGs) were calculated by using the R function FindALLMarkers with Wilcoxon Rank Sum test (Table S7). For the immune cells analysis, cell clusters were assigned through known marker genes as following, Plasma cell_*Mzb1*/*Jchain*/*Derl3*/*Igkn*/*Iglc3*/*Ppib*, Mast cell_*Tpsb1*/*Tpsb2*/*Gata2*/*Ms4a2*/*Cpa3*/*Mcpt2*, B cell_*Cd79a*/*Cd19*/*Bank1*, Dendritic cell (DC)_*Flt3*, Neutrophil_*S100a8*/*S100a9*/*Csf3r*, Monocytes-Macrophage_*Itgam*/ and T cell_*Cd3g*/*Cd8a*/*Cd4*. The proportion of each cell subtypes of T cell or myeloid cells were calculated with two-proportion z-test. The scRNA-seq was performed at the Single Cell Omics Core, School of Biomedical Sciences, Faculty of Medicine, The Chinese University of Hong Kong.

### Bacterial attachment and invasion assay

Live *S. anginosus*, or *S. anginosus*Δ*Tmpc* (MOI =50) was suspended in antibiotic-free DMEM medium supplemented with 10% FBS and co-cultured with a monolayer of gastric epithelial Ges-1 or AGS cells for 2 h. For bacterial attachment and invasion assay, cells were washed by warm PBS for 3 times and lysed with 1% TritonX-100 for 5 min. The cell lysate was collected and stripped in BHI agar for counting attached bacteria numbers with series dilution. For invasion assay, gastric epithelial cells were treated with 200 μM Gentamicin (G4918, Sigma) for an additional 2 h before bacteria CFU counting.

### PCR array

Total RNA was extracted using Trizol reagent (Takara). Complementary DNA (cDNA) was synthesized with PrimeScript RT reagent Kit (RR037A, Takara), and analyzed by the mouse inflammatory response and autoimmunity PCR array (PAMM-077Z; QIAGEN). qPCR primers used for validation are listed in Table S2.

### Western blots

Protein was extracted with Tissue Extraction Reagent (FNN0071, Thermo Fisher Scientific) supplemented with Proteinase inhibitors (Roche) and PhosSTOP (Roche). Image was captured and analyzed by Image-Lab (Bio-Rad, Version 5.2.1). Protein expression level was normalized to β-actin or GAPDH.

### RNA sequencing (RNA-seq) and analysis

Total RNA was extracted from the stomach of *S. anginosus*-treated mice and BHI control mice at 12 months post-infection using Trizol reagent. RNA-seq was performed by BGI Genomics (Shenzhen, China). RNA-seq reads were processed by removing adapters using cutadapt (version 1.18) and mapped on the mouse reference (GENCODE v30) by HISAT2 (version 2.1.0) with the default options. The number of reads mapped to each of genes was counted by using HTSeq (version 0.11.2) with the option-m intersection-nonempty. Gene expression levels were calculated as Fragments per Kilobase of transcript per Million mapped reads (FPKM) using DESeq2.

### Scanning electron microscopy (SEM)

Ges-1 or AGS cells were seeded in sterile coverslips and co-cultured with *S. anginosus* (MOI 50) for 2 h. Next, cells were washed with freshly prepared Sorensen' phosphate buffer (0.1 M, pH 7.2) three times and fixed with 2.5% glutaraldehyde fixative overnight. The fixed coverslips were washed by Sorensen' phosphate buffer 3 times and fixed in 1% osmium tetroxide for 2 h followed by rinsing with distilled water. After dehydration and coating with gold-palladium, specimens were examined by a Cold Field Scanning Electron Microscope (Hitachi SU8010).

### Quantitative PCR of *Tmpc* gene in *S. anginosus*

*S. anginosus* was co-culture with Ges-1 or AGS as described above. After co-culture, bacteria from the supernatant were collected as non-adherent bacteria. Ges-1 or AGS cells were lysed with 0.1% Triton-X100 for 5 mins, then centrifuged with 4000 rpm, 10 mins to collect adherent bacteria. Total RNA of non-adherent and adherent bacteria was extracted by Trizol reagent with prior beads-beating process. For real-time PCR, total RNA was converted to cDNA using PrimeScript RT Reagent kit (RR047B, Takara) and then analyzed with TB-Green Premix Ex Taq (RR420W, Takara), using primer to amplify *Tmpc* gene and reference gene (*Gyrb* and *Rpob*)

### Biotin pull-down assay

Ges-1 membrane protein was labeled with EZ-Link™ Sulfo-NHS-LC-Biotin (2 mM in PBS pH 8.0, 21335B, Thermo Fisher Scientific) for 4 h in 4 °C and then extracted. *S. anginosus* pellets were suspended in Lysis buffer (50 mM Tris-HCl, pH 8.0, 1 mM EDTA, 50 mM NaCl) plus proteinase inhibitors, and protein was extracted by stirring and sonicating with addition of lysozyme (300 μg/mL), 1% (v/v) Triton X-100 and DNase I. *S. anginosus* surface proteins from the supernatant was obtained after centrifugation at 10,000 rpm for 10 min. To perform the binding assay, biotin-labeled Ges-1 membrane proteins were incubated with *S. anginosus* surface proteins and Streptavidin Magnetic Beads (HY-K0208) overnight at 4 °C. Non-labeled Ges-1 cell membrane proteins were used as a negative control. The beads were washed three times with wash buffer (PBS pH 7.4, 0.1% Tween-20) and then boiled with loading dye at 95 °C for 5 min. Boiled samples were subjected to SDS-PAGE and silver staining, and protein bands were identified by mass spectrometry (Table S8).

### GST pull-down assay

To generate recombinant GST-TMPC protein, the *Tmpc* gene (ATCC 33397 strain, Locus Tag EODJBPNH_00792) was cloned into the pGEX-4T-1 vector and transformed into *E. coli* BL21 (DE3). Transformed *E. coli* were grown in ampicillin supplemented LB broth at 37 °C. When optical density reached 0.6∼1.0, 0.5 mM Isopropyl-β-D-thiogalactoside (IPTG) was added to induce protein synthesis at 20 °C overnight. Bacteria pellets were harvested and suspended in PBS-basic lysis buffer (50 mM $NaH_2PO_4$, 150 mM NaCl, pH 7.2, 10 mg/mL Lysozyme, and Proteinase inhibitors). After centrifugation at 10,000 rpm for 30 min, GST-TMPC was purified from the supernatant with a GST-resin. Ges-1 or AGS cell membrane proteins were extracted by Triton X-100 extraction buffer (3 mM

EDTA, 1X PIPES buffer, 1% Triton X-100, Proteinase inhibitors, pH 7.4). Cytoplasmic lysate was removed by pre-treatment with permeabilization buffer (Thermo Fisher Scientific). For GST pull-down, Ges-1 or AGS cell membrane proteins were incubated with or without recombinant GST-TMPC protein overnight at 4 °C, followed by the addition of GST magnetic beads for 4 h. Finally, beads were washed and boiled with 40 μL loading dye. Boiled samples were subjected to SDS-PAGE and silver staining, and protein bands were identified by mass spectrometry (Table S8).

### Co-immunoprecipitation (Co-IP)

For co-IP of Annexin A2, anti-Annexin A2 antibody (60051-1, Proteintech) and Ges-1 or AGS cell membrane protein were incubated with or without recombinant GST-TMPC overnight at 4 °C. Mouse IgG served as negative control. Dynabeads™ Protein G magnetic beads (10004D, Invitrogen) were then added and incubated for 4 h. The beads were washed and boiled with 40 μL loading dye. Boiled samples were subjected to SDS-PAGE and immunoblotted with anti-Annexin A2 or anti-GST (2624, Cell Signaling Technology). Reciprocal GST pull down was also performed with GST-TMPC and recombinant Annexin A2 (AR09353PU-N, Origene).

### Microscale thermophoresis (MST)

MST was performed using the Monolith NT.115 (NanoTemper Technologies). Recombinant Annexin A2 was served as target and labeled with fluorescent by His-Tag Labeling Kit Red-tris-NTA (MO-L018, NanoTemper Technologies). Recombinant GST-TMPC was employed as the ligand. Proteins were prepared in MST buffer (1 X PBS, pH 7.2, 0.05% Tween-20, 2.5 mM DTT). Samples were loaded into NT.115 standard capillaries. Analysis was performed at 25 °C, 40% excitation power, 40% MST power and a constant Annexin A2 concentration of 50 nM. Apparent $K_d$ value was calculated using MO Affinity Analysis v.3.0.5.

### Knockout of *ANXA2* by CRISPR-Cas9

Guide RNAs targeting the human genomic locus of ANXA2 (TCACCTACCTTTGGTCTTGA) was obtained from GenScript and cloned into the lentiCRISPRv2 vector (108100, Addgene). Lentivirus were then generated by co-transfection of lentiCRISPRv2 vector and packaging plasmids in 293T cells. Ges-1 or AGS cells was infected with CRISPR-Cas9-gRNA lentivirus and selected by puromycin for 7 days. Puromycin-resistant clones were isolated and confirmed by western blot.

### Construction of *S. anginosus*Δ*Tmpc*

The upstream and downstream regions of *Tmpc* were amplified using primer (*Tmpc*-up_F/R and *Tmpc*-down_F/R) with chromosomal DNA of *S. anginosus* ATCC 33397 as template. The *Ermb* gene was amplified from p919 plasmid with primer *EMR*_F/R. Gene *Ermb* was inserted into the *Tmpc* gene and cloned into plasmid pUC19 to obtain pUC19-Tmpc::Ermb. *S. anginosus* ($OD_{600}$ =0.02) was incubated with competence-stimulated peptide 1 (CSP-1, 50 ug/mL) and the obtained plasmid DNA (1 ug/mL) for 3 hours at 37 °C and subsequently plated on THY-erythromycin agar. Colonies were picked after 48 hours and screened for successful insertion via PCR. Bacteria chromosome DNA was extracted with QIAamp DNA Mini kit (Qiagen, 51304) and amplified with primer *Tmpc*-F/R to validate the insertion of *Ermb* gene. Primer sequences were listed in Table S2.

## QUANTIFICATION AND STATISTICAL ANALYSIS

### Statistical analysis

The abundance of *S. anginosus* in human gastric biopsies were compared by two-tailed Wilcoxon ranked sum test and *P* value was adjusted by FDR. Pathological scores were compared by Mann-Whitney *U* test or Kruskal-Wallis test. Student's t-test was performed to compare the means between two groups. Multiple group comparison was conducted by one-way analysis of variance (ANOVA). Two-way ANOVA was used for testing the statistical difference of tumor growth curves. A Chi-square ($X^2$) statistic is used for the comparison of proportion of mice with dysplasia between two groups. Statistical analysis was performed using GraphPad Prism 8.2 (GraphPad Software, Inc.). *P* values less than 0.05 are considered significant. Details of statistical analysis were mentioned in each Figure legends.

CellPress
OPEN ACCESS

# Supplemental figures

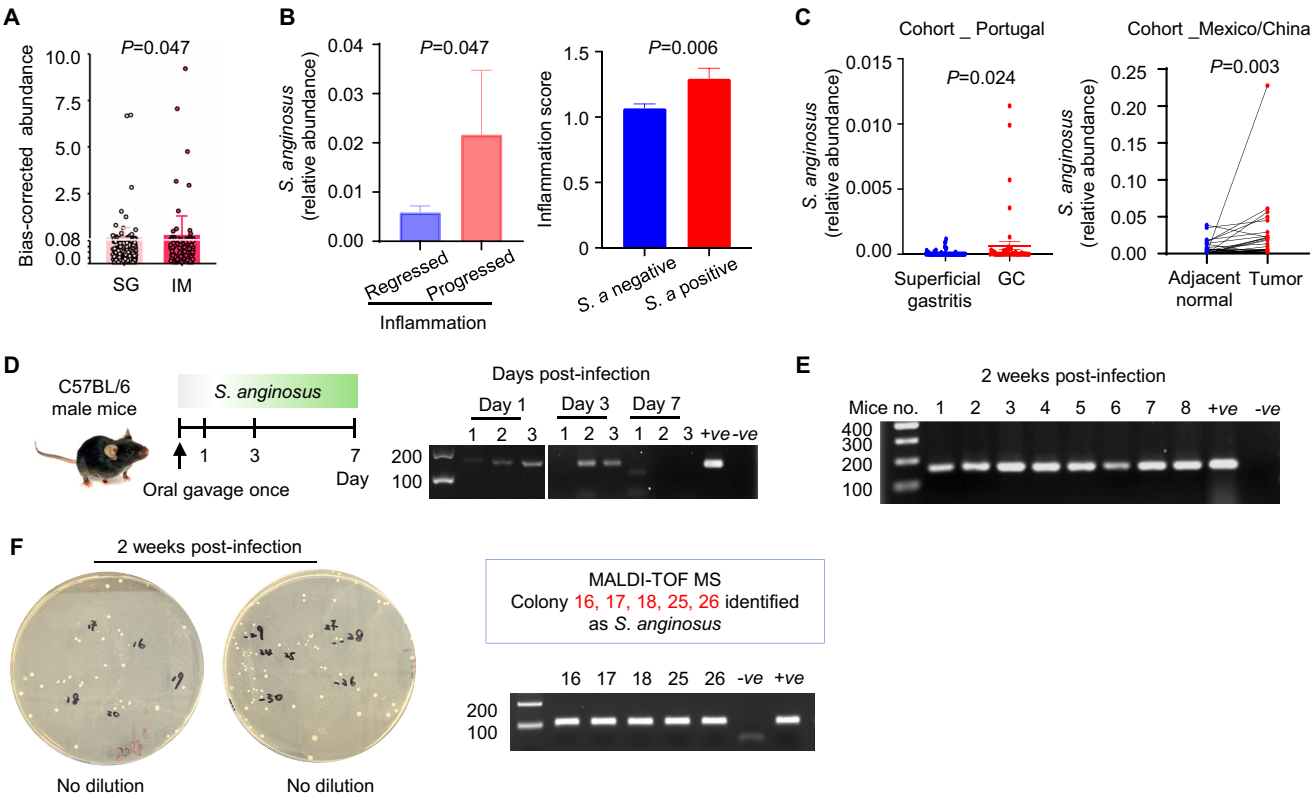


**Figure S1. *Streptococcus anginosus* colonizes gastric mucosa in mice at 2 weeks post-infection, related to Figure 1 and Tables S2 and S3**

(A) The relative abundance of *S. anginosus* in gastric biopsies from SG (N = 302) and IM (N = 153).

(B) The relative abundance of *S. anginosus* in gastric mucosa from patients with regressed (N = 79) or progressed (N = 14) inflammation after *H. pylori* eradication therapy. The inflammation scores in *S. anginosus*-positive (N = 59) and -negative (N = 34) patients.

(C) The relative abundance of *S. anginosus* in superficial gastritis (N = 79) and GC (N = 53) patients in Portuguese cohort (left). The relative abundance of *S. anginosus* in paired gastric tumors and adjacent normal tissues from patients with GC (N = 128) in Mexican/Chinese cohort (right).

(D) PCR detection of *S. anginosus* DNA from mouse stomach at 1 (left DNA gel), 3, and 7 days (right DNA gel) after a single oral gavage of *S. anginosus* ($2 \times 10^9$ CFU). n = 3 for each time point.

(E) PCR detection of *S. anginosus* DNA from the stomach of *S. anginosus*-treated mice at 2 weeks post-infection (oral gavage every 3 days, total 5 doses). n = 8. *+ve*, positive control; *−ve*, negative control.

(F) Bacteria cultured from the stomach of *S. anginosus*-infected mice at 2 weeks post-infection. Colony PCR was conducted to verify MALDI-TOF MS results (Table S3). ANCOM-BC2 (A), Mann-Whitney U test (B and C/left), and Wilcoxon matched-pairs signed rank test (C/right) were used to examine the statistical significance between groups.

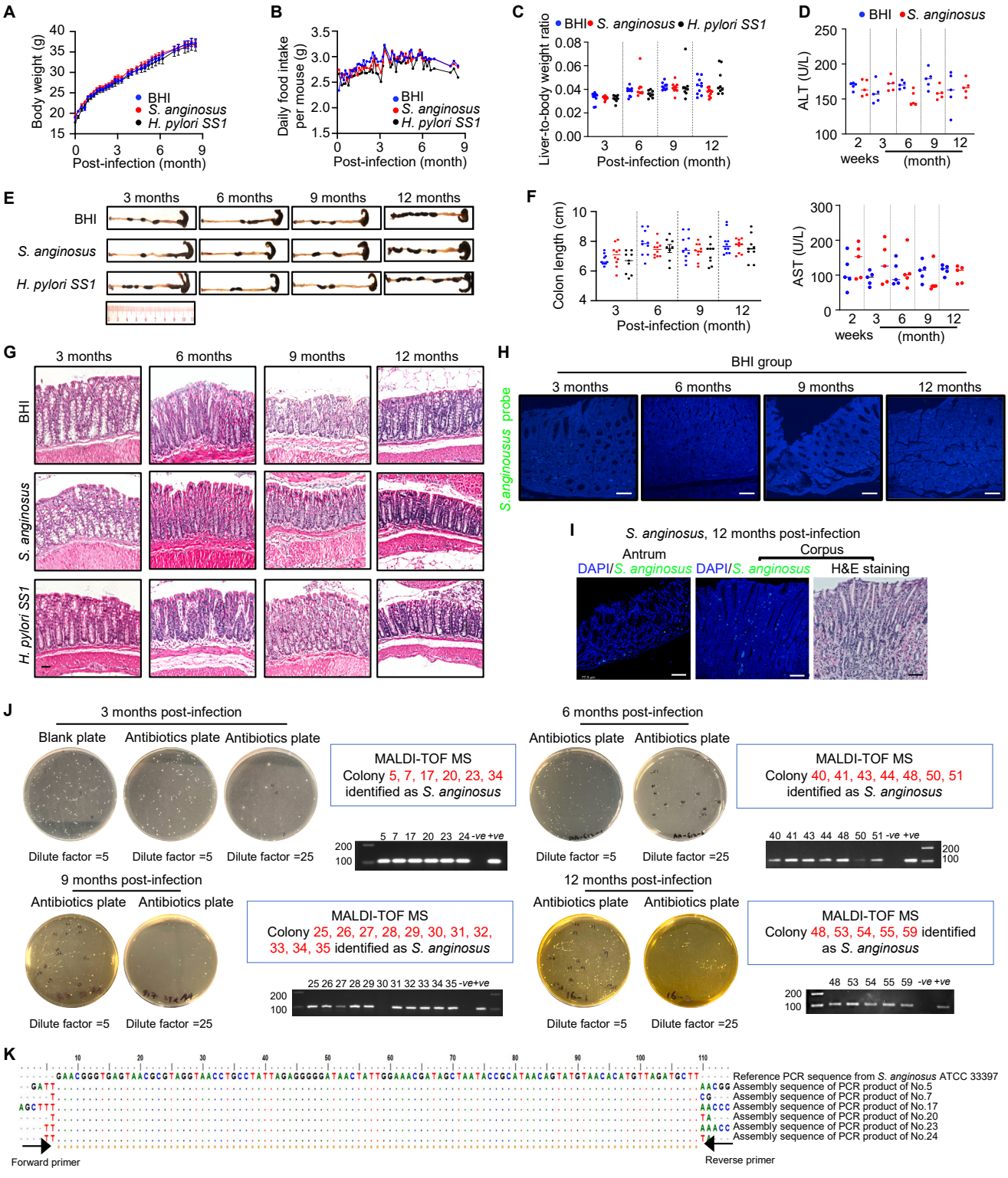


**Figure S2. *Streptococcus anginosus* has no side effects upon long-term infection in mice, related to Figure 2 and Table S3**

(A–C) (A) Body weight, (B) daily food intake, (C) liver-to-body weight ratio of *S. anginosus*- and *H. pylori SS1*-infected mice and BHI control.
(D) Serum ALT and AST levels of *S. anginosus*-infected mice and BHI control.

*(legend continued on next page)*

(E and F) (E) Representative images of colon and (F) colon length of BHI control and *S. anginosus*- and *H. pylori SS1*-infected mice.
(G) Representative H&E staining of colon in BHI control and *S. anginosus*- and *H. pylori SS1*-infected mice; scale bars, 50 μm.
(H) Representative FISH images of gastric tissue sections from BHI control mice (3, 6, 9, and 12 months post-infection) (blue: nuclear, green: *S. anginosus* probe); scale bars, 50 μm.
(I) Representative FISH images of the antrum and corpus region of gastric tissue sections from *S. anginosus*-infected mice (12 months post-infection) (blue: nuclear, green: *S. anginosus* probe); scale bars, 50 μm.
(J) Bacteria cultured from the stomach of *S. anginosus*-infected mice at 3, 6, 9, and 12 months post-infection. Colony PCR was conducted to verify MALDI-TOF MS results (Table S3).
(K) Representative ClustalW multiple alignments of assembly sanger sequence from colony PCR product (3 months post-infection) with reference PCR sequencing from *S. anginosus* ATCC 33397 genome.

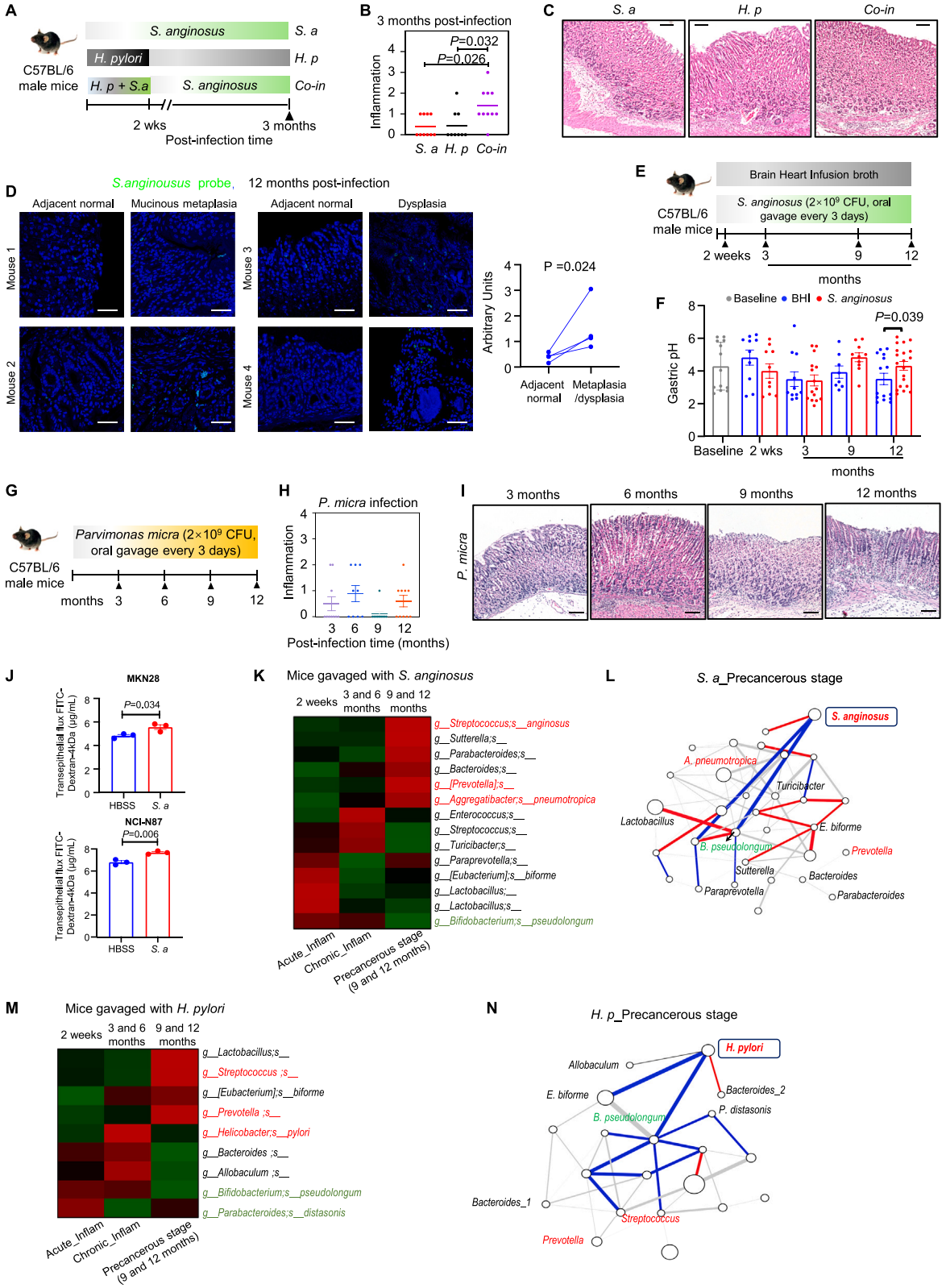


(legend on next page)

**Figure S3. *Streptococcus anginosus* modulates the gastric microbiome composition in mice, related to Figure 3 and Tables S4 and S5**

(A) C57BL/6 male mice were gavaged with *S. anginosus* (n = 10), *H. pylori SS1* (n = 9), or the combination of *H. pylori* plus *S. anginosus* (n = 10).

(B) Histological scores of the stomach.

(C) Representative H&E images of mouse stomach from *S. anginosus*- or *H. pylori SS1* mono-infected mice or co-infected mice; scale bars, 100 μm.

(D) Representative FISH images of adjacent normal, metaplasia, and dysplasia from *S. anginosus*-infected mice (12 months post-infection) (blue: nuclear, green: *S. anginosus* probe); scale bars, 50 μm.

(E) C57BL/6 male mice were gavaged with *S. anginosus* (n = 10 for 2 weeks, n = 15 for 3 months, n = 8 for 9 months, n = 15 for 12 months) or BHI broth (n = 10 for 2 weeks, n = 11 for 3 months, n = 8 for 9 months, n = 15 for 12 months) for 2 weeks, 3, 9, and 12 months.

(F) The changes of gastric pH in response to *S. anginosus* infection compared with BHI control group in mice. Baseline: 8-week-old C57BL/6 mice.

(G) C57BL/6 male mice were gavaged with *Parvimonas micra* (*P. micra*) (n = 10 for 3 months, n = 9 for 6 months, n = 10 for 9 months, n = 20 for 12 months) for 3, 6, 9, and 12 months. The corresponding BHI control group is presented in Figure 2A.

(H) Histological scoring of the stomach in *P. micra*-infected mice. No atrophy, mucinous metaplasia, or dysplasia was found.

(I) Representative H&E images of stomach from *P. micra*-infected mice (3, 6, 9, and 12 months post-infection); scale bars, 100 μm.

(J) *S. anginosus* (MOI = 50) infection led to a marked increase in cell permeability in MKN28 or NCI-N87 monolayers, as determined by FITC-dextran (4 kDa) permeability assay.

(K) Heatmap of differentially abundant bacteria in *S. anginosus* across acute inflammation, chronic inflammation, and precancerous stages. Acute inflammation: 2 weeks post-infection, chronic inflammation: 3 and 6 months post-infection, precancerous stage: 9 and 12 months post-infection.

(L) Ecological network among differentially abundant bacteria in *S. anginosus*-infected mice. Correlations were measured by SparCC method. Line width: correlation strength (red line: positive correlation, false discovery rate [FDR] < 0.05; blue line: negative correlation, FDR < 0.05); node size: bacterial abundance.

(M) Heatmap of differentially abundant bacteria in *H. pylori*-infected mice across acute inflammation, chronic inflammation, and precancerous stages.

(N) Ecological network among differentially abundant bacteria in *H. pylori*-infected mice. Data were shown as mean ± SEM. Each spot represents one subject. The one-way ANOVA (B), two-tailed paired t test (D), Mann-Whitney U test (F), and Student's t test (J) were used to examine the statistical significance among groups.

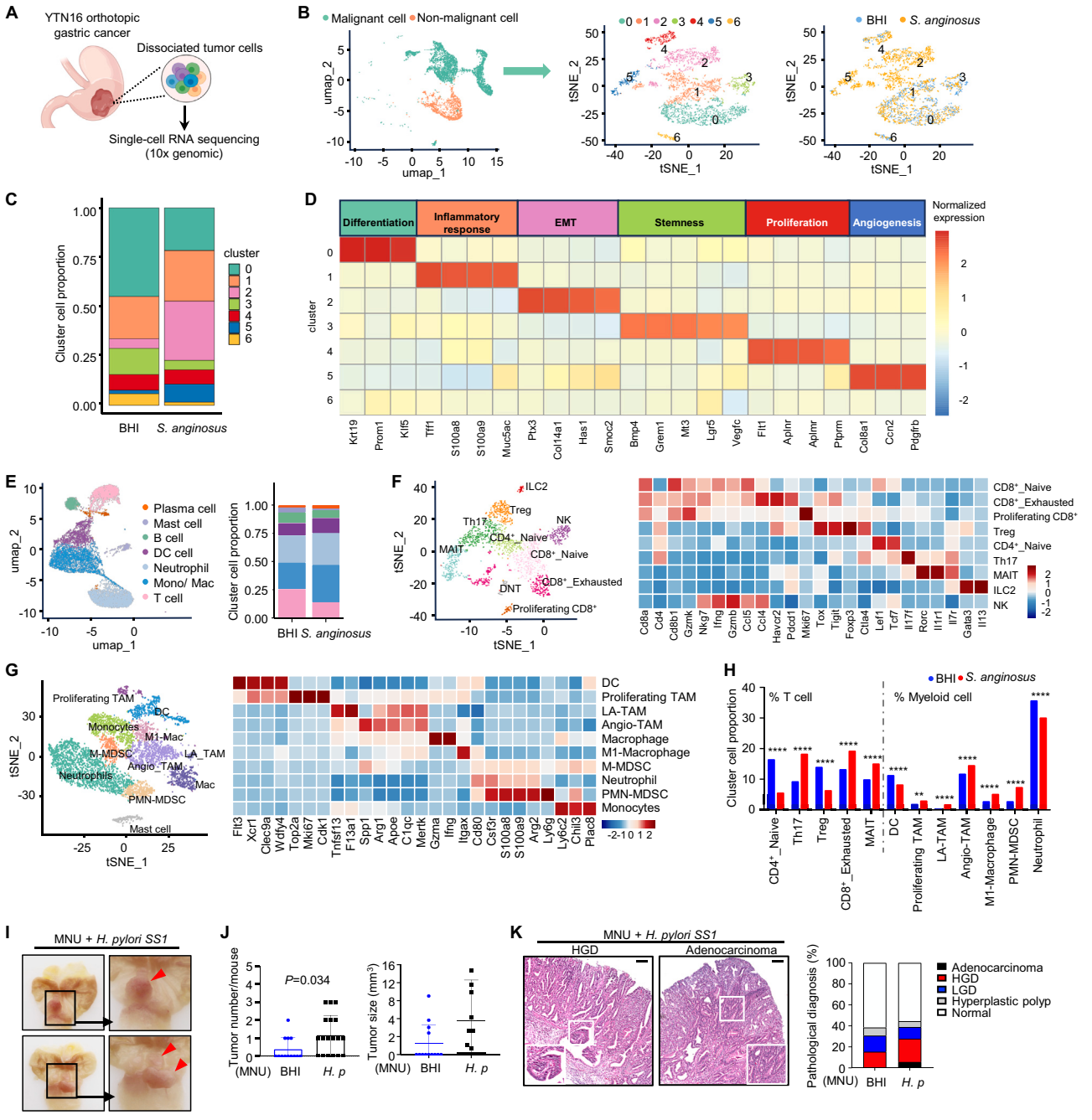


**Figure S4. *Streptococcus anginosus* reshapes gastric tumor microenvironment in mice, related to Figure 5 and Table S7**

(A) Schematic diagram of single-cell RNA sequencing analysis of tumor cells from orthotopic YTN16 tumor model.

(B) Uniform manifold approximation and projection (UMAP) map of 4,836 *Epcam*$^{+}$ epithelial cells from a total of filtered 8,507 single cells in cancer tissues. Non-malignant cells and malignant cells were defined by GC marker genes (*Chga*, *Chgb*, *Pgc*, *Muc5ac*, *Col3a1*, *Cdh17*, *Pdgfrb*, *Cldn4*, *Tff3*, and *Cldn7*). t-Stochastic neighbor embedding (t-SNE) plot showed unsupervised sub-clustering of malignant cells.

(C) The relative proportion of each cluster cell in *S. anginosus*- infected mice and BHI control group.

(D) Heatmap showing the relative expression of marker genes for each cluster cell (y axis).

(E) UMAP of Cd45$^{+}$ immune cells in cancer tissues; fraction of immune cells in BHI and *S. anginosus*-infected groups.

(F) t-SNE plot of T cells. Clusters are labeled with inferred cell types. Heatmap showing marker genes across T cells.

(G) t-SNE plot of myeloid cells. Clusters are labeled with inferred cell types. Heatmap showing marker genes across myeloid cells.

(H) The proportion of significantly altered immune cell types ($p < 0.01$) between BHI and *S. anginosus*-infected groups. p value was calculated by two-proportion *Z* test.

(I) Representative images of the stomach from *H. pylori*-infected mice showed the presence of an adenoma in the antrum site.

*(legend continued on next page)*

(J) Tumor multiplicity and tumor size were higher in *H. pylori*-infected mice compared with BHI control group.
(K) Representative images of H&E staining of stomach from *H. pylori*-infected MNU mice; scale bars, 100 μm. Pathological diagnosis showed a higher proportion of adenocarcinoma and high-grade dysplasia in *H. pylori SS1*-monocolonizaed MNU mice. Data were shown as mean ± SEM. Each spot represents one subject. Mann-Whitney U test (J) was used to examine the statistical significance between groups.

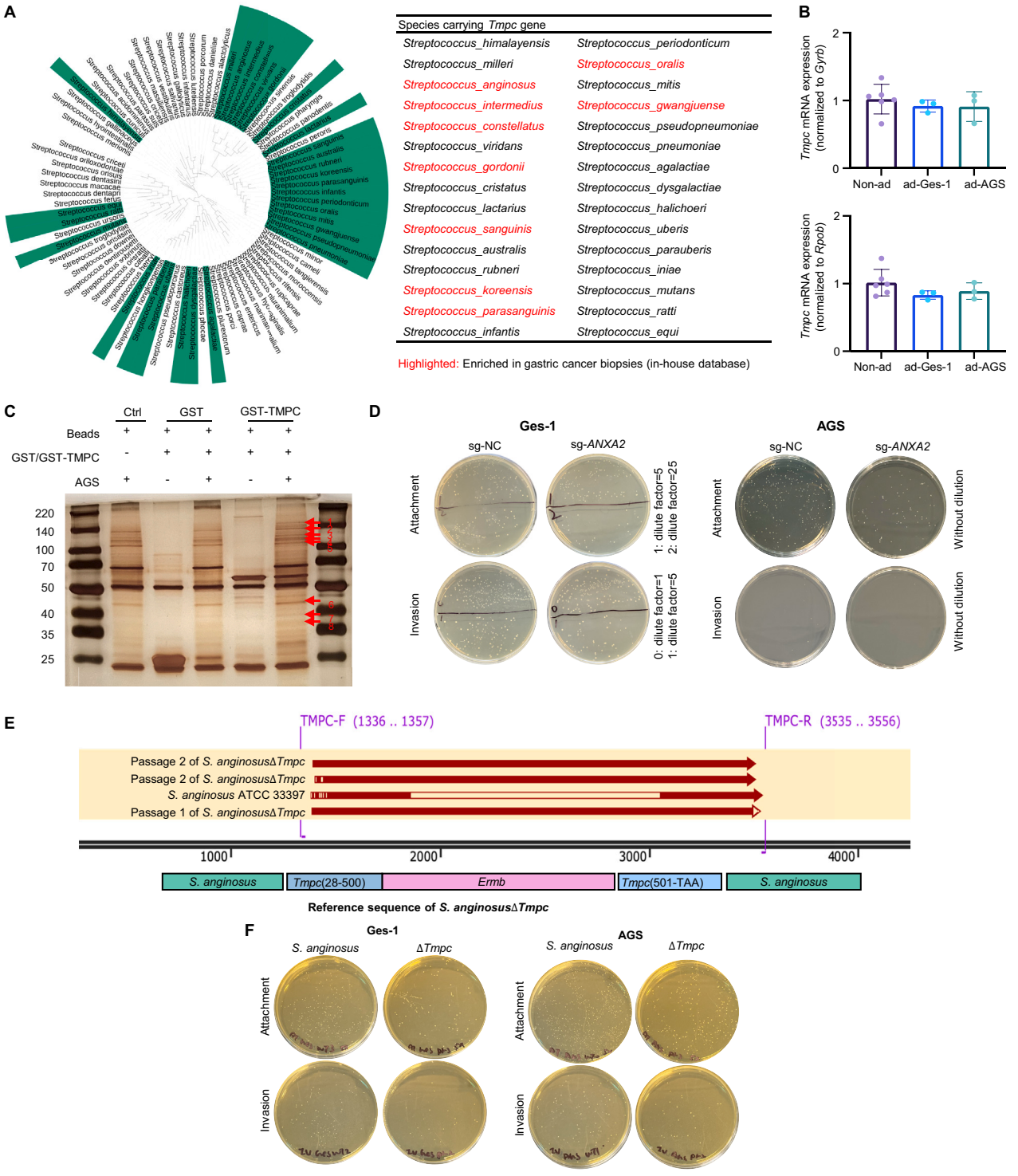


**Figure S5. *Streptococcus anginosus* interacts with gastric epithelial cells through a TMPC-ANXA2 axis, related to Figure 6 and Table S8**

(A) Phylogenetic relationship of *Tmpc* gene. Species carrying *Tmpc* gene from the *Streptococcus* phylogenetic tree are highlighted in green. *Tmpc*-positive *Streptococcus* species (red highlighted in the right table) were enriched in GC (N = 61) compared to non-atrophic gastritis (N = 98) patients according to our in-house database.

(B) The relative mRNA expression level of *Tmpc* gene in *S. anginosus* attached to Ges-1 or AGS cells; non-ad: non-adherent *S. anginosus*, ad-Ges-1: *S. anginosus* adherent to Ges-1, ad-AGS: *S. anginosus* adherent to AGS; reference gene for qPCR: *Gyrb* or *Rpob*.

*(legend continued on next page)*

(C) AGS membrane protein was incubated with GST or GST-TMPC together with GST magnetic beads for GST-pull-down assay. Corresponding bands in GST-TMPC and AGS cell membrane proteins group were subjected to mass spectrometry analysis.
(D) Knockout of *ANXA2* in Ges-1 or AGS cells significantly decreased *S. anginosus* attachment onto and invasion into the epithelial cell.
(E) Sanger sequencing of PCR products of *Tmpc* gene from *S. anginosus*Δ*Tmpc and S. anginosus* ATCC 33397. The red region represents the bases sequence paired to reference genomic of *S. anginosus*Δ*Tmpc*.
(F) *S. anginosus*Δ*Tmpc* showed decreased adhesion and invasion ability compared with *S. anginosus*. Data were shown as mean ± SEM. Each spot represents one subject.

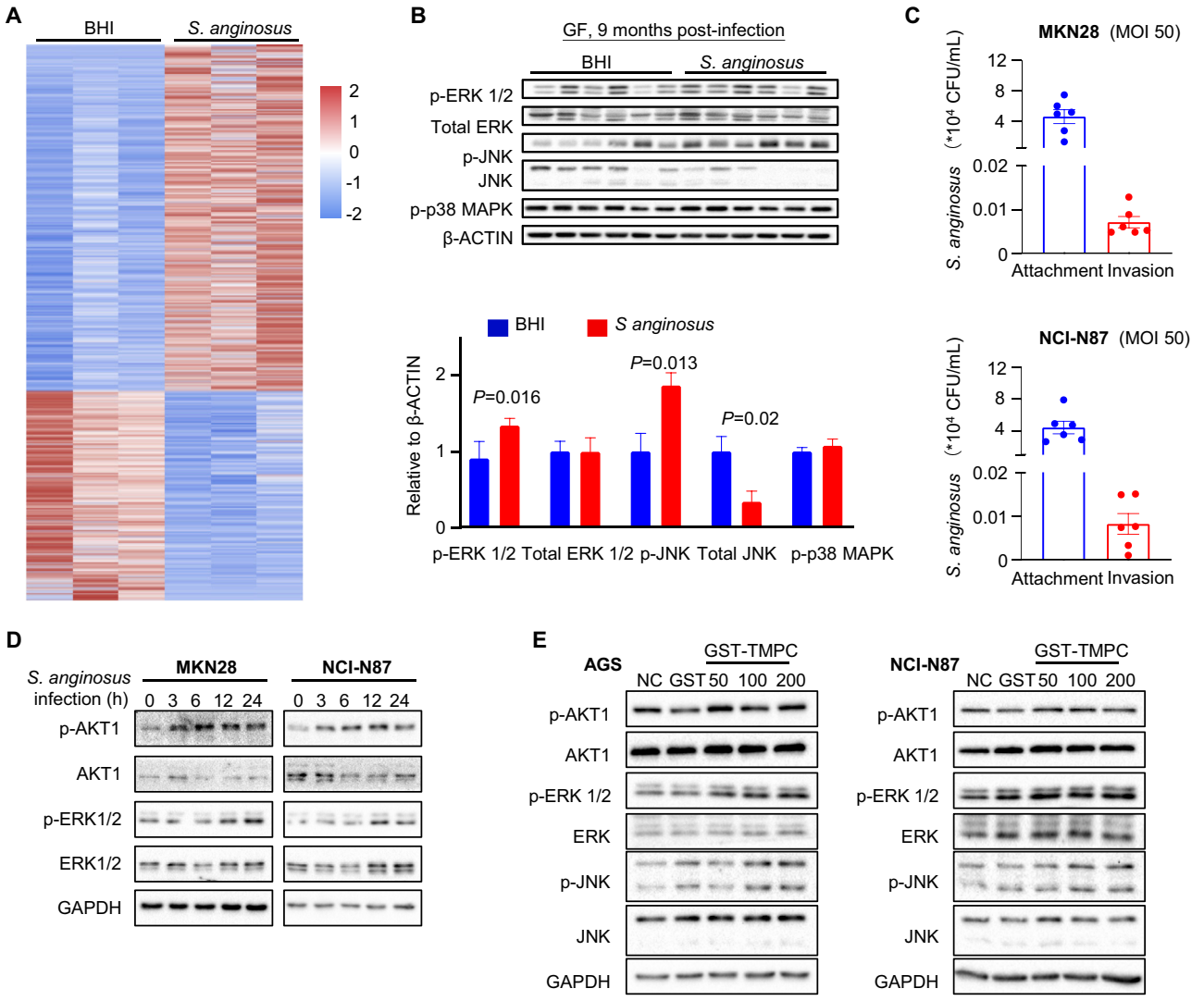


**Figure S6. *Streptococcus anginosus* activates MAPK signaling via TMPC-ANXA2 axis, related to Figure 7**

(A) Heatmap of significantly differentially expressed genes (DEGs) in *S. anginosus*-infected mice compared with BHI control mice. Red: upregulated, blue: downregulated.

(B) Western blot analysis of activation of MAPK pathway in *S. anginosus*-infected mice compared to BHI control group of germ-free mice at 9 months post-infection, with increased p-ERK and p-JNK.

(C) Bacterial attachment and invasion assay showed that *S. anginosus* attached onto and invaded into MKN28 and NCI-N87 cells after co-culture.

(D) *S. anginosus* activated MAPK signaling in MKN28 and NCI-N87 cells after co-culture for 24 h.

(E) Recombinant TMPC (50, 100, and 200 nM) activated MAPK signaling in AGS and NCI-N87 cells after treatment for 24 h. The Student's t test (B and C) was used to examine the statistical significance between groups.